ARTICLES
https://doi.org/10.1038/s41593-018-0262-6
nature neuroscience

Electrical spinal cord stimulation must preserve proprioception to enable locomotion in humans with spinal cord injury

Emanuele Formento[1,2], Karen Minassian[2], Fabien Wagner[2], Jean Baptiste Mignardot[2], Camille G. Le Goff-Mignardot[2], Andreas Rowald[2,3], Jocelyne Bloch[4], Silvestro Micera[1,5,6], Marco Capogrosso[3,6] and Gregoire Courtine[2,4,6*]

Epidural electrical stimulation (EES) of the spinal cord restores locomotion in animal models of spinal cord injury but is less effective in humans. Here we hypothesized that this interspecies discrepancy is due to interference between EES and proprioceptive information in humans. Computational simulations and preclinical and clinical experiments reveal that EES blocks a significant amount of proprioceptive input in humans, but not in rats. This transient deafferentation prevents modulation of reciprocal inhibitory networks involved in locomotion and reduces or abolishes the conscious perception of leg position. Consequently, continuous EES can only facilitate locomotion within a narrow range of stimulation parameters and is unable to provide meaningful locomotor improvements in humans without rehabilitation. Simulations showed that burst stimulation and spatiotemporal stimulation profiles mitigate the cancellation of proprioceptive information, enabling robust control over motor neuron activity. This demonstrates the importance of stimulation protocols that preserve proprioceptive information to facilitate walking with EES.

Spinal cord injury (SCI) has an immediate and devastating impact on movement control. These motor deficits result from the interruption of communication between the brain and spinal cord, depriving the otherwise intact spinal cord executive centers below the injury from essential sources of modulation and excitation to produce movement[1].

EES applied to the lumbar spinal cord immediately enables the executive centers to coordinate a broad range of motor behaviors including standing, walking in various directions, and even running in rodent, feline, and nonhuman primate models of leg paralysis[2–5]. When combined with locomotor training, EES promotes an extensive reorganization of residual neural pathways that restored locomotion without the need of stimulation[2,6].

EES has also been applied to the human spinal cord for several decades but has been less effective. EES induces rhythmic leg movements in people with complete paralysis[7,8], and enables independent stepping when delivered over more than a year of intense rehabilitation[9–11]. EES also enabled volitional activation of paralyzed muscles to initiate isolated leg movements in individuals with motor-complete paralysis[12,13]. However, EES has not restored independent, weight-bearing locomotion in humans with severe SCI, as observed in animal models.

The mechanisms underlying species-specific responses to EES remain enigmatic. This understanding is essential for guiding the development of evidence-based approaches that fulfill the potential of EES to improve recovery after SCI. Evidence from computational models[14,15] and experimental studies[16–18] conducted in animals and humans suggests that EES recruits afferent fibers conveying proprioceptive information. This recruitment leads to the activation of motor neurons through monosynaptic and polysynaptic proprioceptive circuits, and it increases the overall excitability of the lumbar spinal cord. This modulation enhances the responsiveness of spinal circuits to residual descending signals and sensory feedback. In turn, sensory information modulates the reciprocal inhibitory networks in the spinal cord that gate the excitatory drive produced by EES toward functionally relevant pathways. This mechanism enables the generation of muscle activation underlying standing and walking in animal models of paralysis[18].

This conceptual framework implies that sensory information plays a central role in motor-pattern formation during EES. However, this viewpoint does not consider that the recruitment of proprioceptive fibers by EES may interfere with the natural flow of information traveling along the same fibers.

Electrical stimulation triggers bidirectional action potentials (APs) along the recruited fiber. EES would thus elicit orthodromic and antidromic APs that travel to the spinal cord and sensory organs[19–21]. Consequently, we hypothesized that antidromic APs may collide with APs conveying proprioceptive information, preventing its propagation to the brain and spinal cord. The probability of these detrimental interactions is proportional to EES frequency, the firing rate of afferents, and the time required for an AP to travel along the entire length of the fiber. These physiological parameters diverge dramatically between rats and humans. The traveling time of APs along proprioceptive fibers is longer in humans than in rats, and firing rates are lower[22]. The resulting higher probability of

[1]Bertarelli Foundation Chair in Translational NeuroEngineering, Institute of Bioengineering, Swiss Federal Institute of Technology (EPFL), Lausanne, Switzerland. [2]Center for Neuroprosthetics and Brain Mind Institute, School of Life Sciences, Swiss Federal Institute of Technology (EPFL), Lausanne, Switzerland. [3]Department of Medicine, Faculty of Sciences, University of Fribourg, Fribourg, Switzerland. [4]Department of Neurosurgery, University Hospital of Lausanne (CHUV), Lausanne, Switzerland. [5]Neural Engineering Area, Institute of Biorobotics, Scuola Superiore Sant'Anna, Pisa, Italy. [6]These authors jointly supervised this work: Silvestro Micera, Marco Capogrosso, Gregoire Courine. *e-mail: gregoire.courtine@epfl.ch

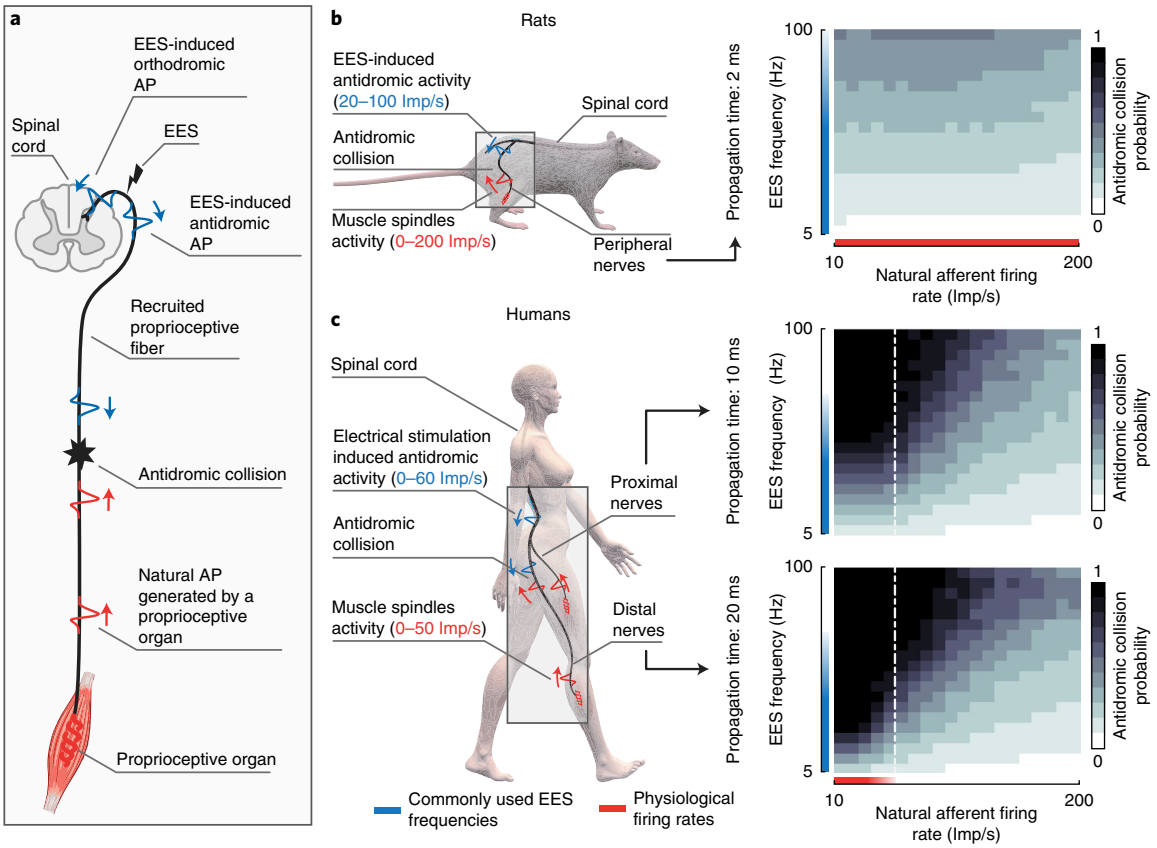

Fig. 1 | Probability of antidromic collisions during EES in rats and humans. a, Schematic illustration of antidromic collisions between EES-induced antidromic APs and natural APs traveling along the recruited proprioceptive afferent fibers. **b**,**c**, Probability for a natural AP to collide with EES-induced antidromic AP (**b**) in the proprioceptive afferent fibers of rats (AP propagation time along the entire length of the fiber: 2 ms) and (**c**) in the proximal and distal proprioceptive afferent fibers of humans (AP propagation times along the entire length of the fiber: 10 and 20 ms, respectively). The probability is calculated as a function of EES frequency and natural firing rate along afferent fibers. EES frequencies that are commonly used to facilitate locomotion in rats and humans are highlighted in blue. Physiological proprioceptive firing rates reported in rats and humans are highlighted in red. Vertical dashed white line highlights the estimated maximum firing rate of human proprioceptive afferents during gait. Imp/s, impulses per s.

collisions between natural and antidromic APs in humans may disrupt sensory information.

Here we hypothesized that this phenomenon explains the limited efficacy of continuous EES in paraplegic individuals compared to rats. We demonstrate that antidromic collisions abolish proprioceptive information in humans, but not in rats. These detrimental interactions restrict the range of EES frequencies and amplitudes that can facilitate locomotion. We report EES strategies that mitigate this issue, demonstrating that EES must preserve proprioception to facilitate walking after SCI.

Results

Antidromic collisions during EES. To study the occurrence probability of antidromic collisions along proprioceptive afferents during EES, we developed computational models of proprioceptive afferents that consider the length of axons innervating proximal and distal muscles, as well as the propagation times of APs. We modeled realistic interactions between natural and EES-elicited APs (Fig. 1a). We thus calculated the probability of antidromic collisions in muscle spindle afferents depending on EES frequency and natural firing rate.

The occurrence probability of antidromic collisions was extremely low in rats, regardless of EES frequency and natural firing rate (Fig. 1b). While delivering EES at frequencies commonly used to enable locomotion in rats (40 Hz[2,23]), this probability never exceeded 20%.

These probabilities were dramatically different in humans. Even relatively low EES frequencies blocked most of the natural proprioceptive signals from reaching the spinal cord. For distal muscles, the occurrence probability of antidromic collisions reached nearly 100% for afferent firing rates of 30 impulses per s at 30-Hz EES frequency (Fig. 1c). The occurrence probability of antidromic collisions was markedly higher along afferents innervating proprioceptors located in distal muscles compared to proximal muscles (Fig. 1c). These results suggest that continuous EES may disrupt proprioceptive information in humans, but not in rats.

EES induces antidromic activity along human afferents. We thus verified whether EES produces antidromic activity along proprioceptive afferents. We recorded the proximal and distal branches of the tibial nerve (mixed nerve), the sural nerve (sensory nerve), and EMG activity from the soleus muscle during continuous EES in two individuals with chronic SCI (Fig. 2a; subjects #2 and #3 in Supplementary Table 1).

We selected an EES configuration that elicited contractions of the soleus and then reduced EES amplitude to elicit a tingling sensation in the corresponding dermatome without visible muscle contraction. In subject #2, each pulse of EES (20 Hz) elicited a weak response in the soleus with a latency of 25 ms, which has been associated with the recruitment of motor neurons via group-Ia afferents[15]. Concurrently, we detected two responses in the proximal branch of the tibial nerve, with latencies of 12.5 and 26.5 ms, and

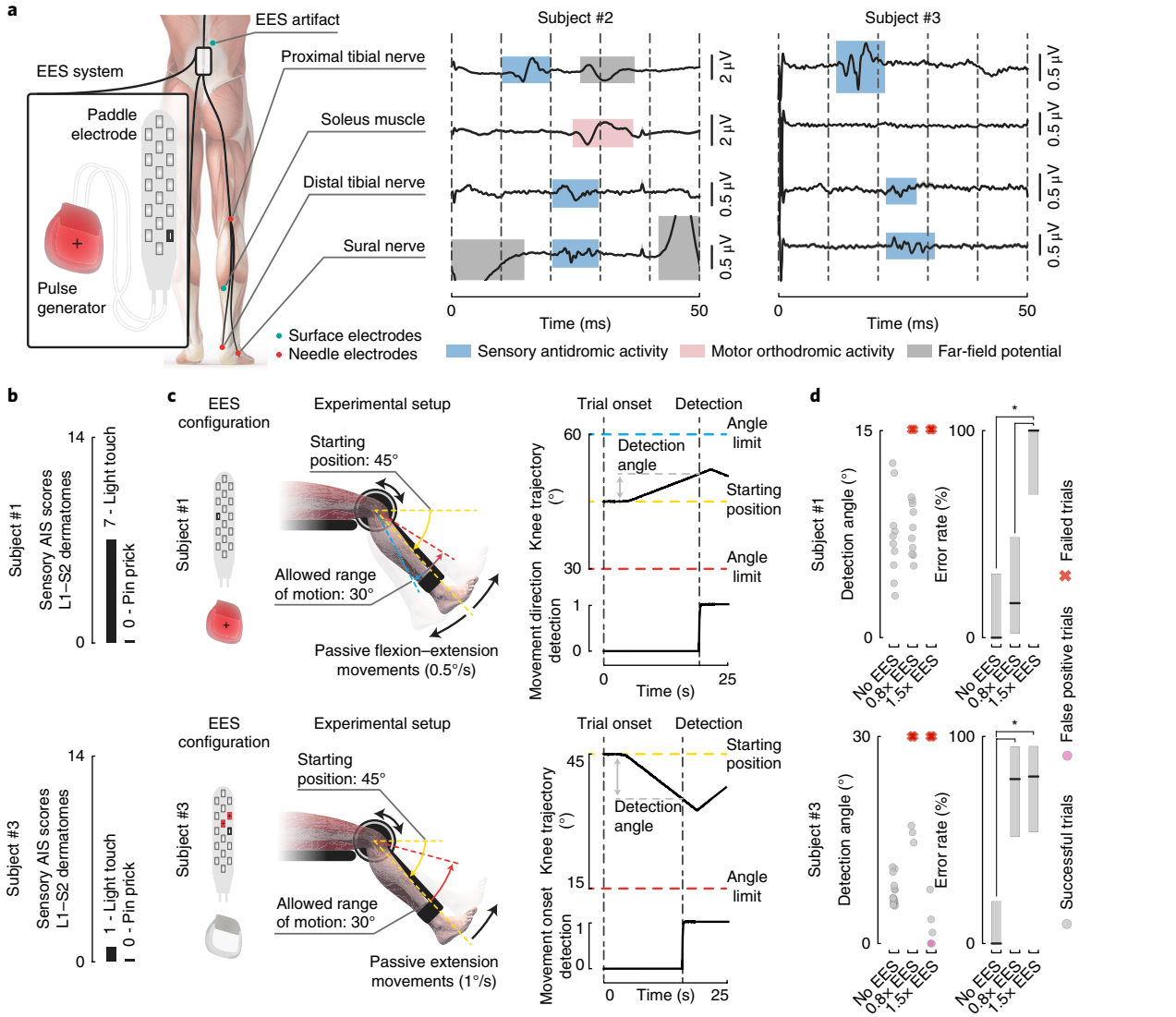

Fig. 2 | EES induces antidromic activity along proprioceptive afferents and disrupts proprioception. a, Recordings of antidromic activity from sensory nerves during EES. Needle electrodes were inserted subcutaneously close to peripheral nerves and surface electrodes over the soleus muscle, as depicted in the scheme. Continuous EES (20 Hz, monopolar stimulation, black cathode and red anode) was delivered for approximately 1 min. Averaged evoked potentials (±s.e.m., $n = 1{,}198$ and $n = 1{,}180$ independent measurements for subjects #2 and #3, respectively). Evoked potentials highlighted in blue, red, and gray were respectively classified as antidromic afferent volleys, efferent orthodromic activity, and far-field potentials (for example, electromyographic activity of nearby muscles), respectively. **b**, Sensory AIS subscores of the lumbosacral (L1–S2) dermatomes for the two subjects that performed the threshold to detection of passive movement (TTDPM) test. AIS, American Spinal Injury Association Impairment Scale. **c**, Setup of the TTDPM test. Top: randomly selected flexion or extension movements were imposed to the knee joint of subject #1. A movement speed of 0.5° s^{-1} and a maximum allowed range of motion of 15° was used. Bottom: subject #3 was not able to perceive movement direction. Hence, only the ability to detect extension movements was assessed. A movement speed of 1° s^{-1} and a maximum allowed range of motion of 30° was used. EES configurations used to target knee flexor and extensor muscles were applied as indicated. **d**, Scatter plots reporting the detection angle and plots reporting the error rate (percentage correct trials ± 95% CI, $n = 32$ and $n = 47$ independent measurements for subjects #1 and #3, respectively) on the TTDPM test performance without EES and when delivering continuous EES (50 Hz) at 0.8× and 1.5× muscle-response-threshold amplitudes. Grey dots, detection angles for successful trials; pink dots and red crosses, false positives and failure to detect movement within the allowed range of motion, respectively. *$P < 0.05$, Clopper–Pearson two-sided non-overlapping intervals.

one response (latency: 21 ms) in the distal branch. The responses induced in the proximal (12.5 ms) and distal (21 ms) branches of the tibial nerve (Fig. 2a) likely resulted from the same neural volley propagating toward the periphery. Since the responses recorded in the distal branch occurred before any motor response, they cannot be attributed to orthodromic efferent activity. These responses corresponded to antidromic afferent volleys. The response (22 ms) recorded in the exclusively sensory sural nerve is compatible with this conclusion. The antidromic recruitment of Aβ afferents is the most probable explanation for this response. In subject #3, each EES pulse elicited a distinct response in both proximal (12.5 ms) and distal (22 ms) branches of the tibial nerve, as well as a response in the sural nerve (22.5 ms). No responses were detected in the soleus muscle. These results indicate that EES elicits antidromic activity along proprioceptive afferents, suggesting that EES interferes with natural sensory information in humans.

EES disrupts kinesthesia. Cancellation of proprioceptive information during EES should alter the conscious perception of joint position and movement velocity. To test this hypothesis, three individuals with a chronic SCI (Supplementary Table 1) completed a threshold to detection of passive movement test. Due to impaired sensory function, only subject #1 and subject #3 could complete the task without EES (Fig. 2b).

Participants sat in a robotic system that imposed a passive isokinetic leg movement (Fig. 2c). They were asked to detect the direction of movement as soon as they could perceive it, but before the knee joint angle reached a predefined amplitude. Without EES, subject #1 detected extension and flexion of the knee with 100% success (median detection angle, 7°; 95% confidence interval (CI), 3.9–11.9°). Without stimulation, subject #3 successfully detected movement onset with 100% success (median detection angle, 6.7°; 95% CI, 5.8–8.4°).

We selected electrode configurations that targeted antagonistic muscles of the knee. We first tested amplitudes that elicited a tingling sensation without producing motor responses (0.8× muscle response threshold). At this intensity and over a broad range of frequencies, continuous EES did not alter subject #1's performance, while detection of movement onset was disrupted in subject #3 (Fig. 2d and Supplementary Fig. 1). At 1.5× muscle response threshold, EES prevented both participants from detecting leg movements. The participants reported a complete loss of awareness of leg position and movement. These psychophysical experiments corroborate our hypothesis that continuous EES disrupts and may even block proprioceptive information in humans. This disruption occurred at EES amplitudes and frequencies commonly used for rehabilitation[8,10–13].

Continuous EES alters afferent modulation of spinal circuits in humans but not in rats. Proprioceptive signals exert a strong influence on the excitability of sensorimotor circuits[24–26]. The cancellation of proprioceptive information during continuous EES in humans should therefore affect the modulation of reflex responses elicited by EES. To test this hypothesis, we studied the modulation of reflex responses elicited by various EES frequencies (5–60 Hz) during passive oscillations of the ankle or knee joint. The participants were seated in a robotic system that imposed passive rhythmic flexion–extension movements of the ankle or knee at a fixed angular velocity and amplitude (Fig. 3a and Supplementary Fig. 2). Continuous EES was delivered with electrode configurations and intensities that induced reflex responses in flexor and extensor muscles of the targeted joint (Fig. 3a and Supplementary Fig. 2).

The rhythmic flexion–extension movements of the joint induced a significant phase-dependent modulation of reflex responses in the mobilized muscles (normalized modulation depth > 0.25; $P < 0.001$ for each frequency, bootstrap test; Fig. 3b–d). However, the extent of this modulation depth depended on EES frequency. Quantification of angle-dependent reflex responses revealed a pronounced monotonic decrease of the normalized modulation depth with EES frequency increments (Fig. 3d).

We performed the same experiments in four lightly anesthetized rats with a contusion SCI that had been implanted with an electrode over the lumbar spinal cord (Fig. 3e–h). Robot-controlled oscillations of the ankle induced a robust modulation of reflex responses (normalized modulation depth > 0.15; $P < 0.001$ for each frequency, bootstrap test). However, we did not detect systematic relationships between EES frequencies and normalized modulation depth (Fig. 3h). Modulation of motor responses was still present at frequencies as high as 100 Hz (Fig. 3g). A linear fit of the median values yielded a slope close to 0 in all rats (median, 0.0003; 95% CI, [−0.0056, 0.0015]; bootstrap test), suggesting a lack of linear dependency between modulation depth and EES frequency. These experiments indicate that continuous EES disrupts the ability of proprioceptive information to modulate the motor output elicited by EES in humans.

Computational models of proprioceptive feedback circuits during locomotion. We next sought to assess the impact of continuous EES on the natural dynamics of proprioceptive feedback circuits during locomotion. Since these interactions cannot be studied in vivo, we synthesized EES properties, proprioceptive feedback circuits, and leg biomechanics into computational models (Fig. 4a). We adapted a previously validated dynamic computational model[18] to the anatomical features of rats and humans. The model includes the minimal proprioceptive neural network responsible for reciprocal activation of antagonist muscles (Fig. 4b). We used species-specific biomechanical and muscle-spindle models to estimate the firing rates of proprioceptive afferents during locomotion. This afferent activity was used to steer the neural networks (Fig. 4c).

We first studied the impact of EES on the activity of proprioceptive afferents. To model increments in EES amplitude and frequency, we scaled up the number of recruited afferent fibers and the rates of both orthodromic- and antidromic-induced activities. In rats, EES did not alter the modulation depth of proprioceptive information (Fig. 4d). In striking contrast, the same parameters of EES dramatically disrupted the modulation of proprioceptive information in humans. At frequencies as low as 40 Hz, antidromic APs abolished the sensory information conveyed by each electrically stimulated fiber. The residual modulation of proprioceptive information resulted solely from the activity of nonrecruited afferent fibers. The percentage of erased proprioceptive information was directly proportional to EES amplitude (Fig. 4d).

We then evaluated the impact of this cancellation on the ability of EES to steer reciprocal activation of motor neurons innervating antagonist muscles during locomotion. Continuous EES delivered excitation to Ia-inhibitory interneurons and motor neurons. In rats, the modulation of Ia-inhibitory interneurons driven by the natural proprioceptive information led to a reciprocal activation of antagonist motor neurons during the stance and swing phases of gait (Fig. 5a). Increasing EES frequency or amplitude resulted in higher firing rates of motor neurons, but only during their natural phase of activity .

In the human model, antidromic collisions dramatically disrupted the dynamics of the neural network (Fig. 5b). At low frequency and low amplitude, continuous EES steered the reciprocal activation of antagonist motor neurons, as observed in rats. With higher stimulation parameters, the cancellation of proprioceptive information prevented phase-dependent modulation of Ia-inhibitory interneurons. The resulting imbalance between antagonist pools of Ia-inhibitory interneurons led to a profound asymmetry in the excitatory drive delivered to motor neurons. Extensor motor neuron pools became overactive while flexor motor neuron pools received strong inhibition (Fig. 5b).

Together, these results suggest that only a narrow range of EES parameters could be exploited to enhance the excitability of the human spinal cord without compromising the critical role of proprioceptive information in the production of locomotion. Therefore, the degree of controllability over human motor neurons may be very limited compared to that achievable in rats.

Limited facilitation of locomotion in humans compared to rats. We then evaluated the impact of EES frequencies and amplitudes on leg muscle activity during locomotion in rats and humans. Rats with a clinically relevant contusion SCI[6] and EES electrodes ($n = 4$ rats) were positioned bipedally in a bodyweight support system over a treadmill (Fig. 6a). Continuous EES (40 Hz) induced robust locomotor movements of the otherwise paralyzed legs (Fig. 6b). As previously reported[3,18,27], increases in EES frequencies (20–80 Hz) led to a linear modulation of leg muscle activity, which gradually adjusted kinematic features such as step height (Fig. 6b,c).

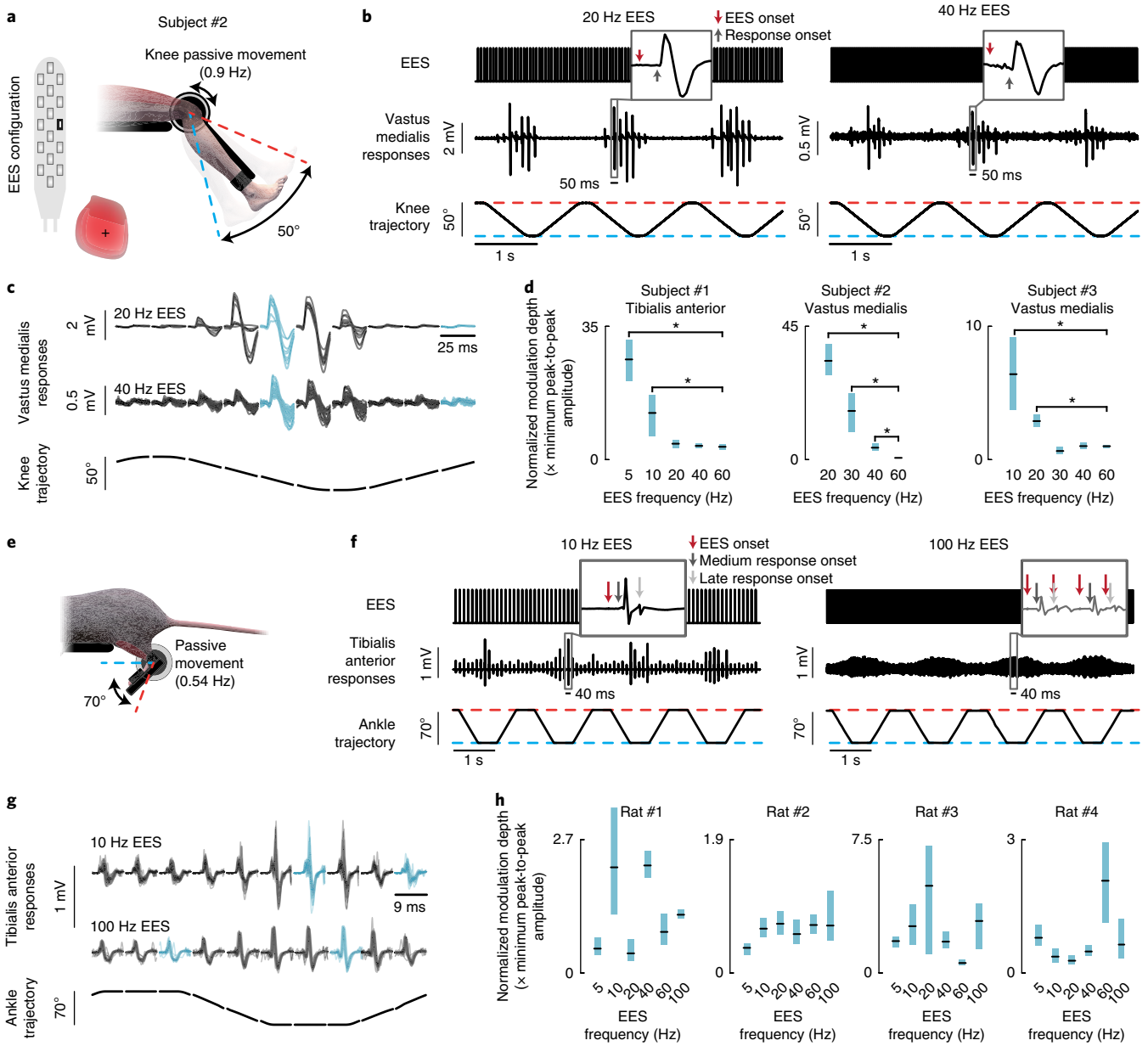

Fig. 3 | Effect of EES on the natural modulation of proprioceptive circuits during passive movements. a, Configuration of the experimental setup for subject #2. The subjects were secured in a robotic system that moved the ankle or knee joint passively within the reported range of motion. EES electrodes were configured to target a muscle that underwent stretching cycles during the selected joint movement (red). Configurations of the experimental setup for subjects #1 and #3 are reported in Supplementary Fig. 2. **b**, Plots showing EES pulses, EMG activity of the vastus medialis, and changes in knee joint angle during passive oscillations of the knee for two different EES frequencies (20 and 40 Hz) in subject #2; similar results were obtained in subjects #1 and #3. The same plots for 60 Hz are reported in Supplementary Fig. 2. Rectangular windows, muscle responses induced by a single pulse of EES; red and gray arrows, the onset of the stimulation pulse and of the muscle response, respectively. **c**, The joint oscillation cycle was divided into ten bins of equal durations, during which muscle responses were extracted and regrouped. Superimposed muscle responses are displayed for each bin for two EES frequencies (subject #2). Muscle responses used to compute the normalized modulation depth are depicted in light blue. **d**, Plots reporting the median and 95% CI of the normalized modulation depth, for each EES condition tested and for each subject. The CI was bootstrapped (10,000 iterations) over $n = 2{,}344$, $n = 1{,}080$, and $n = 2{,}820$ muscle responses, respectively, for subjects #1, #2, and #3. Low frequencies of stimulation often induced spasms in the muscles. Consequently, subjects #2 and #3 could not be tested with EES frequencies below 20 and 10 Hz, respectively. $^*P < 0.05$, two-sided bootstrap test. **e**–**h**, Configuration of the experimental setup for rats with severe contusion SCI (250 kdyn) and results, following the same conventions as in **b**–**d** for human subjects. Results in **f** and **g** are for rat #1; similar results were obtained for all rats. The CI in **h** was bootstrapped (10,000 iterations) over $n = 1{,}834$, $n = 1{,}982$, $n = 1{,}984$, and $n = 1{,}983$ muscle responses, respectively, for rats #1, #2, #3, and #4.

The three human participants with SCI were supported by a gravity-assist[28] that provided trunk support to facilitate stepping on a treadmill (Fig. 6d). Using rails located on each side of the treadmill, subject #1 (60% body weight support) and subject #2 (70% body weight support) were able to take some steps on the moving treadmill belt and produce alternating activation of antagonist leg muscles without EES. However, this muscle activity did not translate into functional movements, as both feet dragged along the treadmill belt at the end of stance. The amplitude of leg movements remained limited. Continuous EES (40 Hz, 3–9 mA)

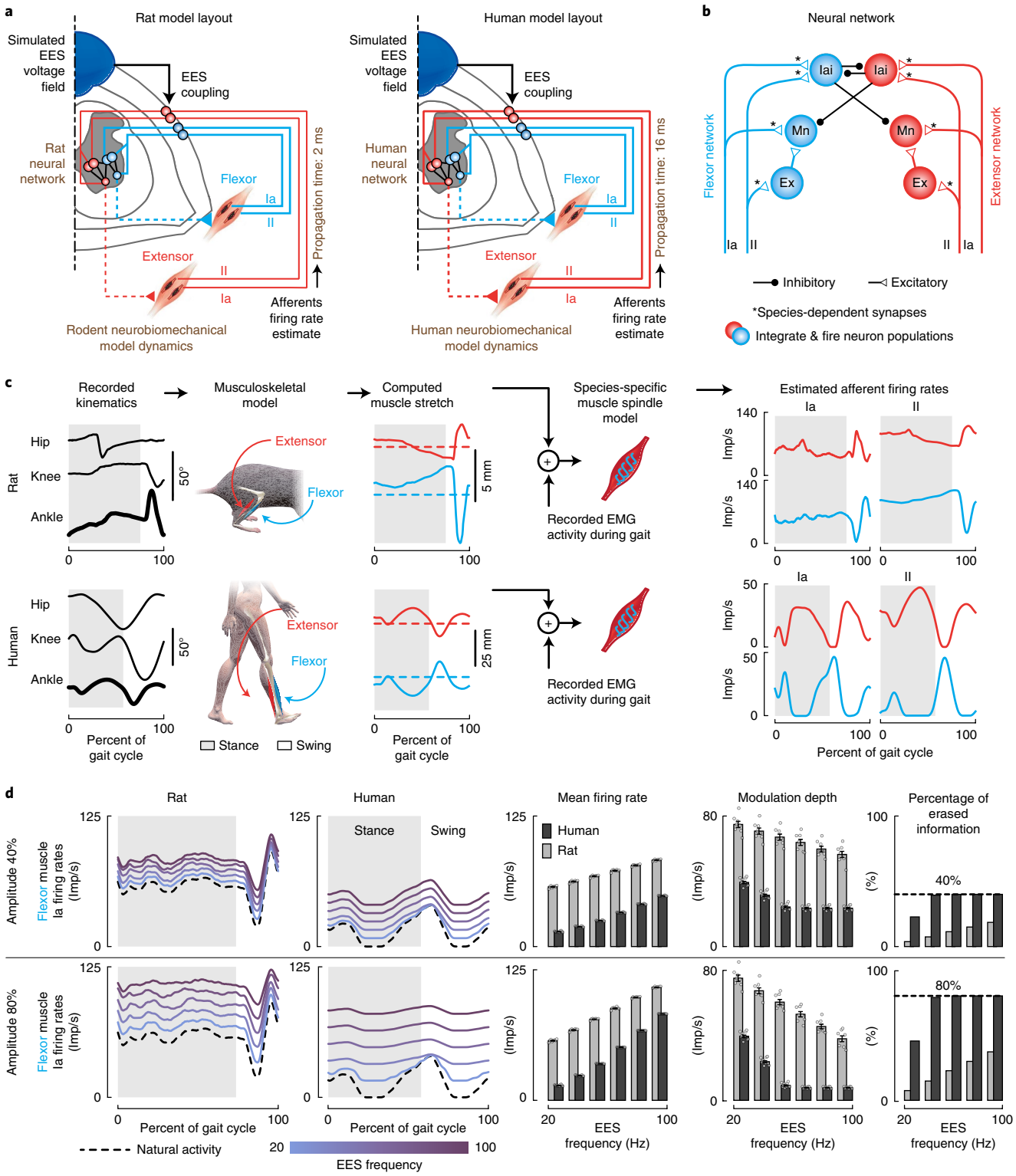

Fig. 4 | Impact of continuous EES on proprioceptive afferent firings during locomotion in rats and humans. a, Layout of the computational models built for rats and humans. Components highlighted in brown are tuned to match the anatomical and physiological features of rats vs. humans. **b**, Spiking neural network model of muscle spindle feedback circuits for a pair of antagonist muscles. Mn, motor neuron; Ex, excitatory interneurons; Iai, Ia-inhibitory interneurons. Synapses highlighted with an asterisk (*) are tuned to match the known properties of human and rat synapses. **c**, Estimated stretch profiles and afferent firing rates of ankle flexor and extensor muscles over an entire gait cycle in rats (top) and humans (bottom). Similar results were obtained for $n = 8$ gait cycles in rats and $n = 11$ gait cycles in humans. **d**, Impact of EES on the predicted natural firing rate profiles of group-Ia afferents innervating a flexor muscle of the ankle during locomotion in rats (left) and humans (right). From left to right: averaged firing rate profiles of the simulated population of afferent fibers over one gait cycle, mean afferent firing rate (±s.e.m., $n = 8$ gait cycles in rats, $n = 11$ gait cycles in humans), modulation depth of afferents firing rate profiles (mean ± s.e.m., $n = 8$ gait cycles in rats, $n = 11$ gait cycles in humans), and total amount of sensory information erased by EES. Results are reported over a range of EES frequencies. Top and bottom: results for EES amplitudes recruiting 40% (top) or 80% (bottom) of the entire population of modeled group-Ia afferents.

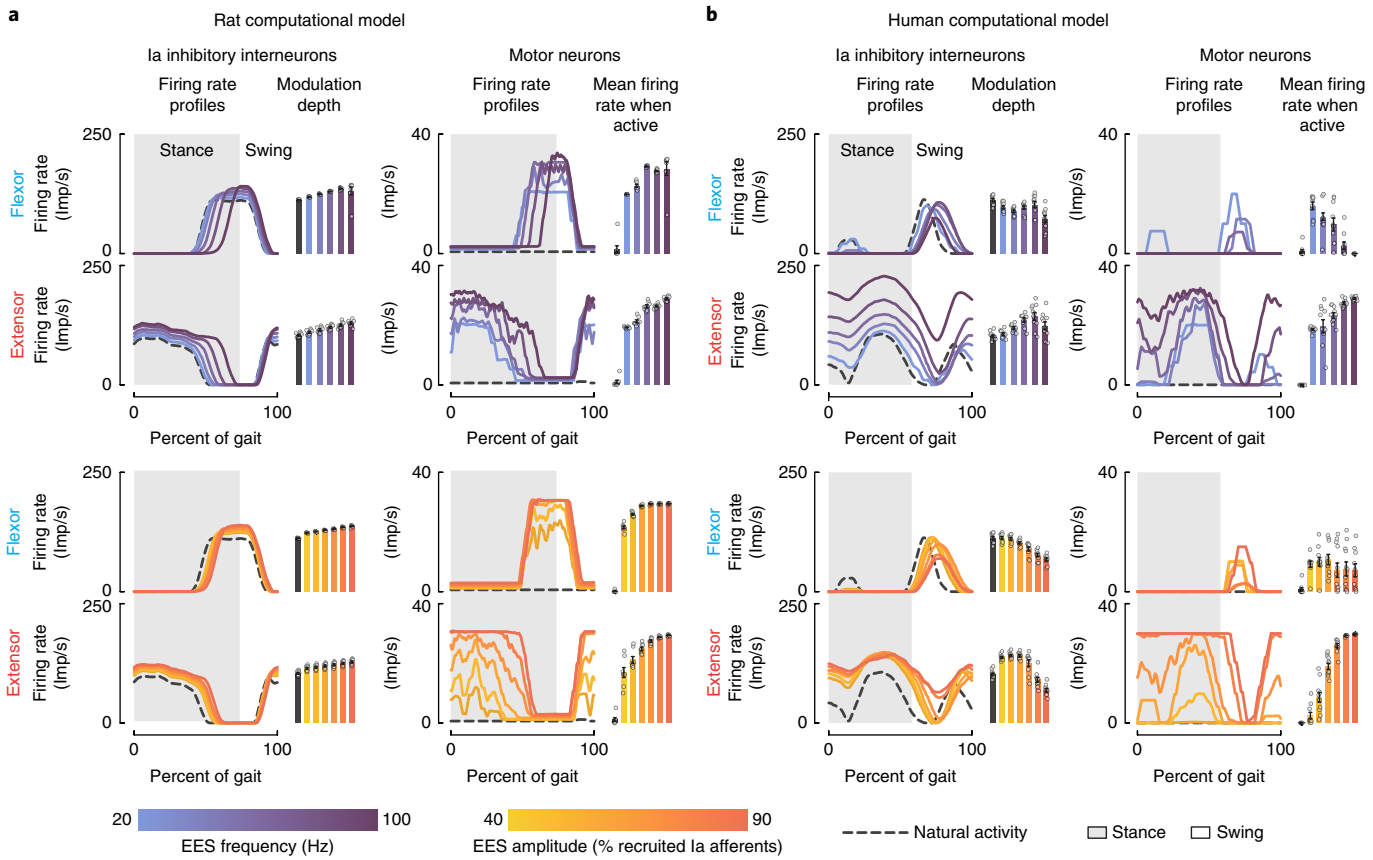

Fig. 5 | Interactions between EES and muscle spindle feedback circuits during locomotion in rats and humans. a,**b**, Impact of EES on the modeled natural activity of Ia-inhibitory interneurons and on the activation of motor neurons during locomotion in rats and humans. Left: average firing rate profiles and modulation depth of the Ia-inhibitory interneuron populations embedded in the flexor or extensor part of the neural network (mean ± s.e.m., $n = 8$ gait cycles in rats, $n = 11$ gait cycles in humans). Right: average firing rate profiles and mean firing rate during the active phase for flexor and extensor motor neurons embedded in the flexor or the extensor neural network (mean ± s.e.m., $n = 8$ gait cycles in rats, $n = 11$ gait cycles in humans). Impacts of EES frequencies and amplitudes are reported in the top and bottom panels, respectively. EES amplitude was set to a value recruiting 65% of the modeled Ia afferents when EES frequency was scaled up, while EES frequency was set to 60 Hz when the amplitude was increased.

facilitated leg muscle activity and kinematic features (Fig. 6e,f and Supplementary Figs. 3 and 4). Contrary to what we observed in rats, however, this facilitation was insufficient to enable coordinated, weight-bearing locomotion. Subject #3 exhibited flaccid paralysis of all leg muscles. Continuous EES increased muscle activity, but failed to produce consistent modulation of this activity to produce stepping (Supplementary Fig. 5). All participants reported a complete loss of limb position awareness during continuous EES, which affected their ability to coordinate the timing of locomotor movements.

Consequently, we sought to augment muscle activity with increases in EES frequency or amplitude. From optimal EES parameters, increases in frequency or amplitude did not improve stepping. The amplitude of EMG activity scaled up in flexor muscles, but this increase was associated with a concomitant decrease in extensor muscles, even leading to a complete suppression of extensor muscle activity (Fig. 6e,f and Supplementary Figs. 3 and 4). EES often induced co-activation of antagonist muscles, with abnormal bursting activity in flexor muscles during stance. Co-activation of muscles induced a sensation of stiff legs, reflected in the reduced range of motion of leg joints (Fig. 6e,f and Supplementary Figs. 3 and 4). These results are consistent with our simulations, indicating that the range of useful EES parameters are too narrow to enable robust locomotion in humans without training, thus providing a plausible explanation for interspecies differences in the therapeutic impact of continuous EES.

Spatiotemporal EES protocols may remedy the limitations of continuous EES. We next exploited our computational model to identify stimulation strategies that may remedy the identified limitations of continuous EES. We reasoned that, to avoid disrupting the natural network dynamics, the temporal and spatial structure of EES should encode the profile of proprioceptive feedback information. We surmised that the amplitude and frequency of the stimulation targeting a specific muscle should be proportional to the instantaneous firing rate of the proprioceptive afferents originating from the sensory organs located in this muscle. Due to the continuous match between the proprioceptive afferent activity and the stimulation profile, EES would augment the overall excitation delivered to the targeted motor pool without compromising the information conveyed by the proprioceptive afferents. Targeting antagonist motor pools with their specific stimulation profile would contribute to maintaining the modulation of reciprocal inhibitory networks that is necessary to facilitate walking with EES. In turn, we hypothesized that adjusting the amplitude and frequency used to configure the stimulation profiles would enable controlling the activity of motor neurons.

We implemented this stimulation strategy in the computational model. We constructed stimulation profiles that combined the natural modulation of primary and secondary proprioceptive afferents (group Ia, group II, and group Ib; Fig. 7a,b) from the homonymous muscles. We did not explicitly model Golgi tendon organs, although Ib afferents are also recruited with EES and provide strong excitation

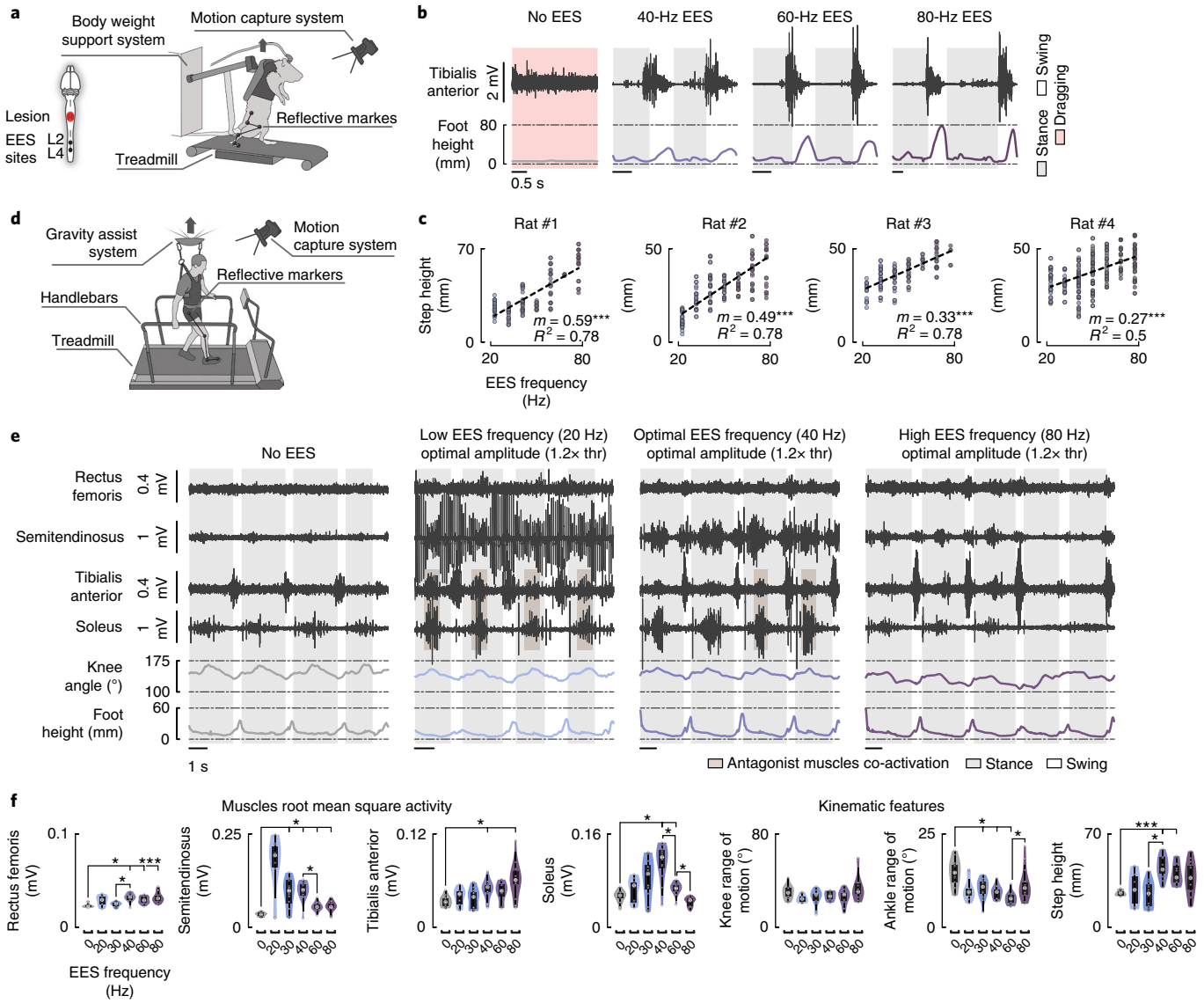

Fig. 6 | Impact of EES frequencies on muscle activity and leg kinematics during locomotion in rats and humans. a, Experimental setup in rats. Rats with a severe contusion SCI were positioned in a robotic body weight support system located above a treadmill. Continuous EES was applied over L4 and L2 segments through chronically implanted electrodes secured over the midline of the dorsal spinal cord. **b**, EMG activity of the tibialis anterior muscle and foot height trajectory over two gait cycles without EES and with EES delivered at 40 Hz, 60 Hz, and 80 Hz in rat #1; similar results were obtained for rats #2, #3, and #4. **c**, Scatter plots reporting step heights at different gait cycles for the tested EES frequencies ($n = 111$, $n = 139$, $n = 101$, and $n = 231$ gait cycles, respectively, for rats #1, #2, #3, and #4). Dashed lines show linear regressions between the EES frequency and the step height. Slope (m) and R^2 are reported. $^{***}P < 0.001$, two-sided Wald test, slope $\neq 0$. **d**, Experimental setup in humans. Subjects were positioned in a gravity-assist system that provided personalized forward and upward forces to the trunk. Subjects were asked to step on the treadmill while holding the handlebars, since they were not able to step independently with the hands free. **e**, EMG activity of flexor (semitendinosus and tibialis anterior) and extensor (rectus femoris and soleus) muscles spanning the right knee and ankle joints, together with the changes in the knee ankle angles and foot elevation over 4 gait cycles without EES and with EES delivered at 20 Hz, 40 Hz, and 80 Hz in subject #1; similar results were obtained for 49 gait cycles (analyzed in **f**). EES amplitude was set to 1.2× the muscle response threshold (thr). Note the opposite modulation of EMG activity in extensor and flexor muscles with increase in frequencies together with co-activation of flexor with extensor muscles. **f**, Violin plots reporting root mean square activities of the recorded muscles, ranges of motion of knee and ankle angles, and step heights at different gait cycles for subject #1 ($n = 77$ gait cycles). Small gray dots, individual data points; large white dots, medians of the different distributions. Boxes and whiskers report interquartile ranges and adjacent values, respectively. $^{*}P < 0.05$, $^{***}P < 0.001$, two-sided Wilcoxon rank-sum test with Bonferroni correction for multiple comparisons. The same results are reported for subjects #2 and #3 in Supplementary Figs. 4 and 5.

during locomotion[29]. Because of the close correlations between Ib afferent firings and homonymous muscle activity[30], the EMG envelope was used as a surrogate for the firing profile of Ib afferents.

Simulations revealed that this strategy erased proprioceptive information to a similar extent as continuous EES (Fig. 7c). Due to the continuous match between the natural proprioception and stimulation profile, however, the proprioceptive signals reaching the spinal cord contained the same amount of information. Naturally generated APs annihilated by antidromic collision were replaced by EES-produced orthodromic APs. While the percentage of erased information increased with EES amplitude (Fig. 7c), the depth of proprioceptive afferent modulation was preserved or even

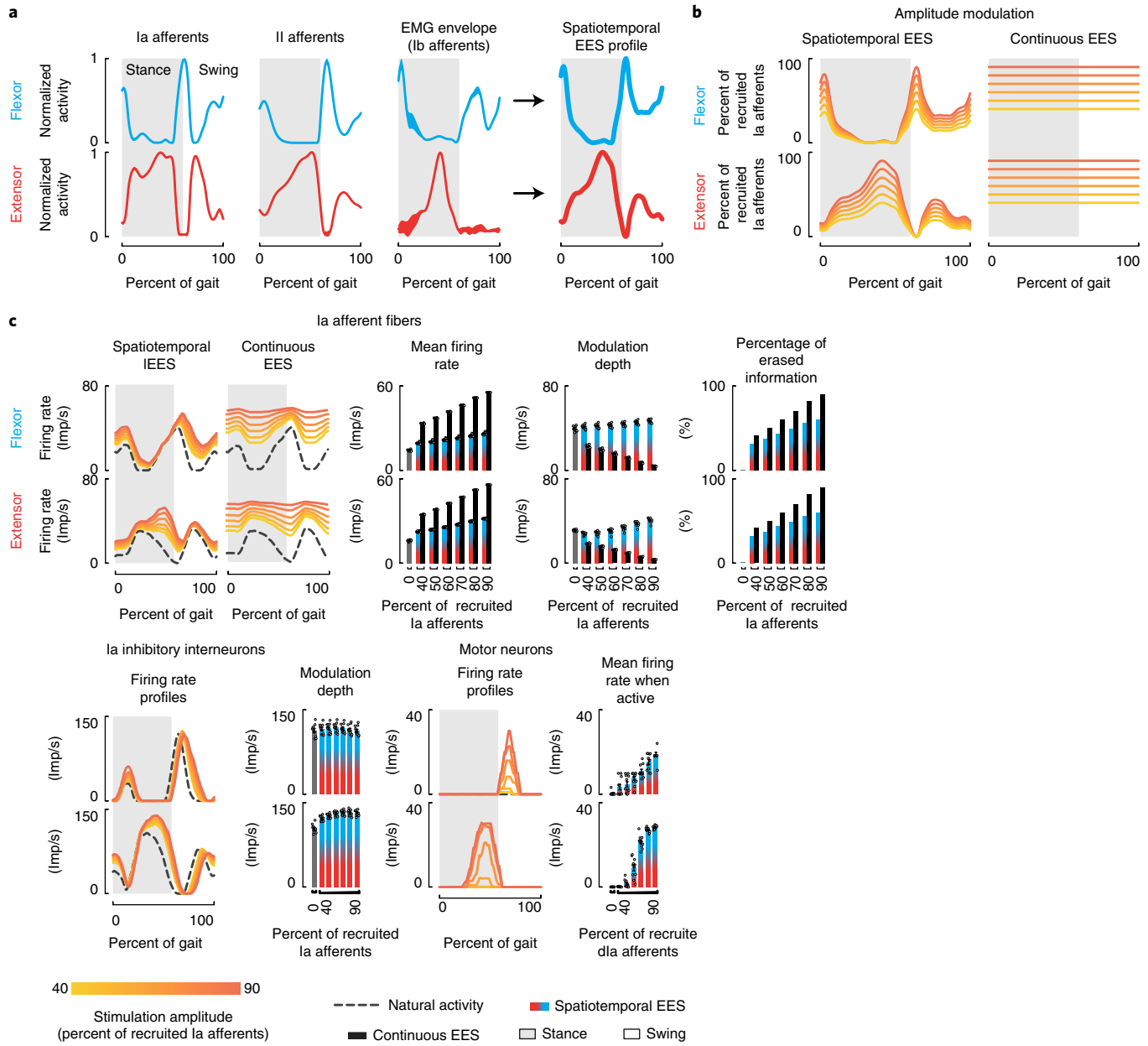

Fig. 7 | Spatiotemporal EES protocols encoding proprioceptive sensory information. a, Estimation of spatiotemporal stimulation profiles that match the natural flow of proprioceptive information generated from flexor and extensor muscles of the ankle during gait. From left to right: estimated averaged firing rate profiles of group-Ia, group-II, and group-Ib (equivalent to the muscle activity) afferents over a gait cycle, and the sum of these profiles that yielded the estimated stimulation profiles. **b**, Percentage of primary afferents that are recruited when applying the estimated spatiotemporal stimulation profile and during continuous stimulation. **c**, Impact of the estimated spatiotemporal stimulation profile on the modulation of muscle spindle feedback circuits from flexor and extensor muscles, from left to right: group-Ia afferent firings, bar plots reporting the averaged mean firing rate and modulation depth of primary afferents (mean ± s.e.m., $n = 11$ gait cycles), overall percentage of sensory information erased by EES, modulation of Ia-inhibitory interneurons, and motor neuron activity (mean ± s.e.m., $n = 11$ gait cycles). For comparison, the impact of continuous EES on the group-Ia afferent firings is also reported. Results of simulations are shown for a range of EES amplitudes. Conventions are as in Fig. 5.

increased for higher stimulation amplitudes. Consequently, the stimulation artificially drove reciprocal modulation of Ia-inhibitory interneurons, as would natural proprioception during walking (Fig. 7c). Scaling up EES amplitude led to a proportional increase in the firing rates of proprioceptive afferents, which augmented the excitation delivered to motor neurons. Since this excitation was restricted to the active phase of each motor neuron pool, increasing EES parameters enabled a linear modulation of motor neuron firing rates (Fig. 7c). These results suggest that encoding the profile of proprioceptive afferent activity into the spatiotemporal structure of EES protocols may expand and refine control over the amplitude of motor neuron activity, while also reinforcing the modulation of reciprocal inhibitory networks, thereby enhancing the facilitation of walking compared to continuous EES.

High-frequency, low-amplitude EES alleviates the disruptive effects of continuous EES. We finally explored whether alternative strategies based on continuous EES could alleviate the cancellation of proprioception. We sought to design a stimulation strategy that minimizes the amount of erased proprioceptive information

during continuous EES while providing high postsynaptic excitation to motor neurons. Each Ia afferent synapses onto every motor neuron that innervates the homonymous muscle[31,32]. Moreover, high-frequency stimulation of nerve afferents leads to a temporal summation of excitatory postsynaptic potentials (EPSPs) delivered to the targeted cell[33–35]. We concluded that recruiting a limited number of Ia afferents with a stimulation burst of low amplitude but high frequency could theoretically deliver the same excitation to motor neurons as recruiting a large number of Ia afferents with single pulses of high amplitude. We thus hypothesized that each pulse of EES could be replaced by a high-frequency, low-amplitude burst of EES that would provide the same overall excitation to motor neurons while reducing the overall amount of erased proprioceptive information. Indeed, while proprioceptive information traveling along the recruited fibers would still be blocked by the stimulation, the reduced number of electrically recruited afferents would ensure that a large amount of fibers remained able to convey sensory signals to the spinal cord. Finally, the excitation delivered to motor pools could then be controlled by adjusting the interburst interval.

We tested the hypotheses underlying this stimulation strategy using computer simulations with multicompartmental motor neuron models and realistic distribution of Ia afferent synaptic contacts (Fig. 8a). As predicted, the temporal summation of EPSPs elicited by high-frequency, low-amplitude bursts of stimulation enabled recruiting the same number of motor neurons as single pulses of high-amplitude EES (Fig. 8b).

To validate these results experimentally, we conducted electrophysiological experiments in five rats. Figure 8c shows motor responses recorded in the tibialis anterior during single pulses and single bursts of EES (25-ms duration, frequencies: 100–1,000 Hz) at increasing amplitudes. Compared to single pulses, high-frequency burst stimulation decreased the threshold to elicit a motor response by 39.8% (s.e.m.: ±4.4%). The largest reductions were obtained toward 500 Hz (s.e.m.: ±54.8 Hz). Decreases in EES burst amplitude led to increased latencies of motor responses, suggesting that more pulses were necessary to recruit motor neurons through the temporal summation of EPSPs (Fig. 8d).

The pulse generator implanted in the participants could generate waveforms with a maximum frequency of 125 Hz. However, the simultaneous delivery of interleaved waveforms (2-ms hard-coded delay) enabled the configuration of single bursts composed of 4 pulses delivered at 500 Hz. This feature allowed us to evaluate the concept of high-frequency EES in humans. As observed in rats, high-frequency bursts of EES required markedly reduced stimulation amplitudes to elicit a motor response, compared to single pulses (Fig. 8e,f).

We implemented this stimulation strategy in the computational model. We delivered EES bursts, consisting of 5 pulses at 600 Hz, with a stimulation amplitude recruiting 20% of all primary afferents. Compared to continuous EES, this stimulation reduced the amount of erased proprioceptive information (Supplementary Fig. 6). Decreasing the time between each EES burst led to a proportional increase in the excitation delivered to motor neurons. These results suggest that high-frequency, low-amplitude stimulation protocols may alleviate the detrimental impact of continuous EES on the modulation of proprioceptive feedback circuits in humans.

Discussion

We have accumulated evidence that the antidromic recruitment of proprioceptive afferents during continuous EES blocks the propagation of naturally generated proprioceptive signals to the brain and spinal cord. Computer simulations suggest that this cancellation of proprioceptive information disrupts the natural modulation of reciprocal inhibitory networks that is essential to produce alternating recruitment of antagonist motor pools during locomotion. Consequently, only a narrow range of EES parameters can facilitate movement in people with SCI, which is insufficient to enable locomotion without extensive rehabilitation[10,11]. Computer simulations guided the identification of EES protocols that not only preserve proprioceptive information but also enable a robust control over motor neuron activity. Here we discuss the significance of these results, stress the dramatic consequences of the transient proprioceptive deafferentation during EES, and envision the avenues for translating these new stimulation protocols clinically.

EES erases proprioceptive information in humans, but not in rats. Evidence indicates that EES primarily recruits large-diameter afferents within the posterior roots[15]. These afferents originate from proprioceptive organs, which sense changes in muscle length and tension, and to a lesser extent, from mechanoreceptors within the skin. EES elicits orthodromic APs along the recruited afferents that mediate the therapeutic effects of the stimulation[18]. However, we show that EES also induces antidromic APs that travel in the opposite direction. Indeed, recordings of peripheral nerve activity identified antidromic volleys propagating toward sensory organs in response to EES in humans. Previous studies documented the presence of antidromic APs traveling along the sensory fibers of the sciatic, peroneal, and sural nerves in rats, dogs, nonhuman primates, and humans in response to EES applied to thoracic segments[19–21]. Here we establish the high occurrence of antidromic APs when EES targets the lumbar posterior roots.

We reasoned that EES-induced antidromic action potentials may collide with APs conveying proprioceptive information. The annihilation of APs following these collisions is due to the refractory period of Ranvier's nodes. Computer simulations predicted a high occurrence probability of these collisions along the recruited afferents when EES is delivered at frequencies commonly used in human studies to facilitate movements after SCI. Due to the longer length and therefore longer propagation time of APs along human proprioceptive afferents, the incidence of these collisions is considerably higher than in rats. These results suggest that EES may partially cancel proprioceptive information in humans.

To assess this possibility, we conducted experiments that highlighted the consequences of these collisions on the integration of proprioceptive information in the brain and spinal cord of humans. First, we found that the delivery of continuous EES abolishes the conscious perception of leg position and displacement. Second, we showed that proprioceptive information drives the modulation of spinal circuits during movement and that the cancellation of this information during continuous EES disrupts this modulation.

Over the past two decades, EES has been applied to thousands of people to alleviate pain and to improve motor function after SCI[8–13,36]. For pain treatments, low-intensity stimulation is applied at the thoracic level. Consequently, there was no obvious loss of sensation in the legs during EES. For SCI, the participants exhibited no or limited sensation in the legs, which may explain why this unexpected cancellation of proprioception information remained unnoticed. However, this phenomenon has far-reaching implications for the development of a therapy to restore locomotion with EES. Indeed, this transient proprioceptive deafferentation not only alters the conscious control of movement and the modulation of spinal circuits with EES, but may also compromise the reorganization of residual descending pathways during rehabilitation enabled by EES.

Proprioceptive information must be preserved to enable locomotion with EES. Bipedal locomotion requires the integration of information from a multiplicity of sensory modalities, of which proprioception may be the most important. Proprioceptive information gives rise to a conscious perception of limb positions[37] that plays a critical role during walking[38,39]. For example, the sudden loss of proprioception induces severe gait deficits[40,41]. Individuals with chronic proprioceptive loss can learn to compensate using

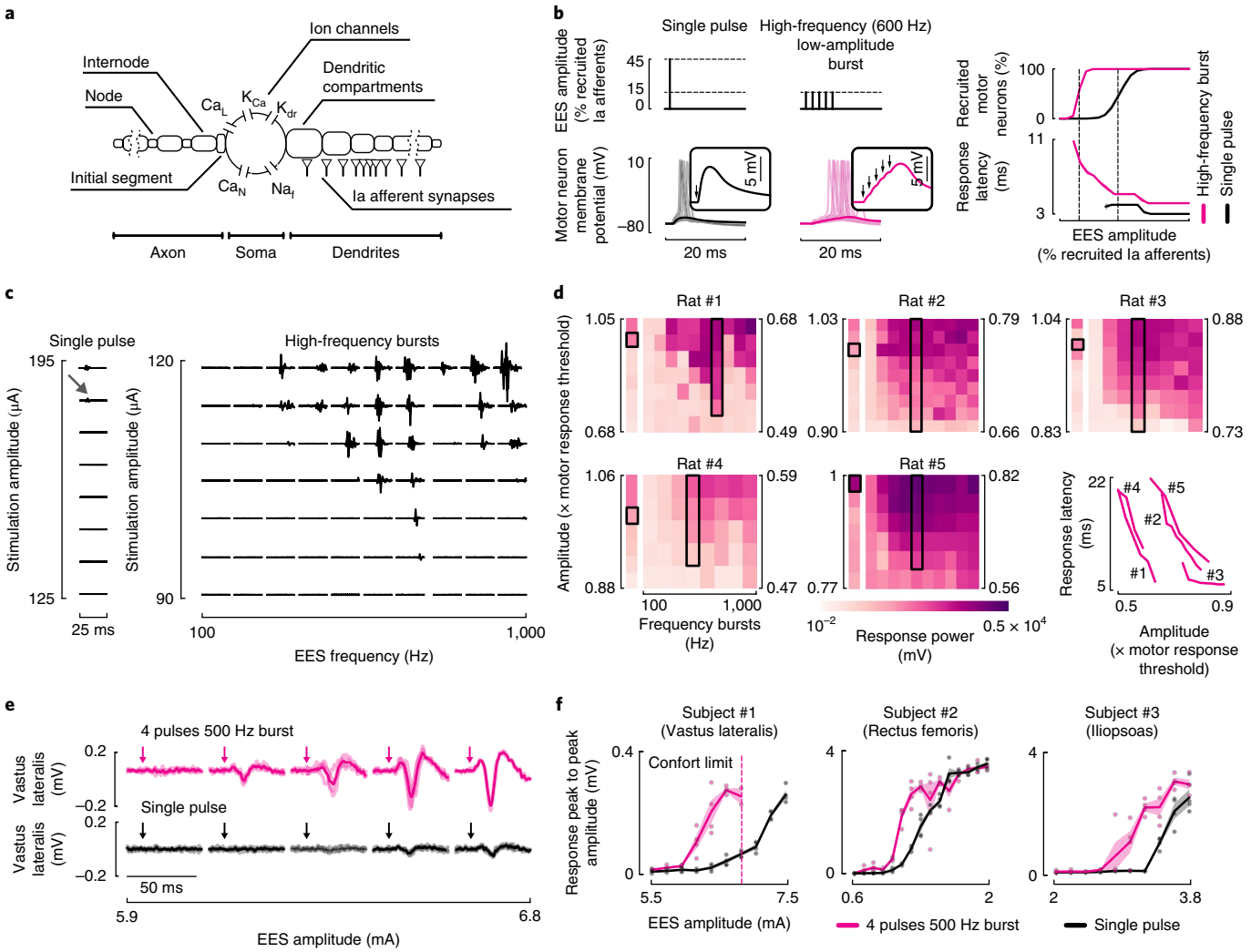

Fig. 8 | High-frequency, low-amplitude bursts of EES recruit motor neurons through temporal summation of EPSPs. a, Multicompartmental model of alpha motor neurons with realistic strengths and distributions of group-Ia synaptic contacts. Ca_L, K_{Ca}, K_{dr}, Ca_N, and Na_f represent the conductances modeling, respectively, the L-type Ca^{2+}, Ca^{2+}-activated K, delayed rectifier K^+, N-type Ca^{2+}, and nonlinear fast Na^+ channels of the motor neurons soma. **b**, Simulations showing the responses of motor neurons to a single pulse of EES at an amplitude recruiting 45% of the afferent population, and to high-frequency bursts (5 pulses, 600 Hz) at an amplitude recruiting 15% of the afferent population. Windows, zoomed view of the motor neuron membrane potential depolarizations in response to the pulses of EES (arrows). Right: plots showing the percentage of recruited motor neurons and the average (mean ± s.e.m., $n = 5$ simulations with different random seed) latency before the onset of an action potential. **c**, Responses recorded from the tibialis anterior muscle following a single pulse of EES (left) and high-frequency bursts of EES (right) applied to rat L2 spinal cord with severe contusion SCI over a range of amplitudes and burst frequencies (rat #1; data for all rats shown in **d**). Gray arrow, responses induced by single-pulse EES at the motor response threshold amplitude, emphasizing the need to deliver high amplitudes to elicit responses with single pulses compared to high-frequency bursts. **d**, Heatmaps representing the average power of motor responses ($n = 4$) to single pulses (column, left) and high-frequency bursts (matrix, right) of EES over a range of EES amplitudes and bursts frequencies, for 5 rats. EES amplitude is reported as a multiple of motor response threshold, with amplitude corresponding to the response highlighted by the black box. The highlighted column corresponds to the bursts with the frequency inducing the largest motor responses. Right: latencies of motor responses elicited by EES bursts with the frequency highlighted in the black boxes, at increasing amplitudes. **e**, Motor responses recorded from the vastus lateralis muscle induced by single pulses (bottom) and high-frequency bursts of EES for different stimulation amplitudes (subject #1). Shaded curves represent single trials ($n = 4$ for each amplitude tested); solid curves represent the average responses. Arrows indicate the onset of the stimulation. **f**, Plots representing the response peak-to-peak amplitudes (mean ± s.e.m., $n = 4$ for each amplitude tested) as a function of EES amplitude, for both single pulses (black) and high-frequency bursts (pink) and for each subject. In subject #1, EES amplitudes > 7 mA elicited uncomfortably powerful contractions and were thus not tested.

other sensory modalities, especially vision[41]. While this adaptation enables them to walk, the associated cognitive load obliges them to rely on a wheelchair for daily life. All our participants reported a loss of limb position awareness during EES. Consequently, this disruption of proprioception strongly limits the clinical relevance of continuous EES to support locomotion during daily living activities in people with SCI.

In addition to its integration in the brain, the information derived from proprioceptive organs is distributed throughout the spinal cord via a dense network of afferent feedback circuits that directly activate motor neurons and shape motor pattern formation during locomotion. Signals from muscle spindles and Golgi tendon organs determine the timing of phase transitions, substantially contribute to leg motor neuron pool recruitment, and coordinate the adaptions

of leg movements to unpredictable perturbations and task-specific requirements[42–45]. Our results suggest that these key mechanisms of motor control are obstructed during continuous EES. Moreover, the interruption of descending pathways reinforces the critical role of these proprioceptive feedback circuits, which become the primary source of control for motor pattern formation[46]. For example, the integration of proprioceptive information enables the spinal cord to coordinate locomotion across a broad range of speeds, loads, and directions in animal models of complete SCI[23]. The disruption of proprioceptive information during EES would severely degrade this ability of the spinal cord to coordinate motor pattern formation after SCI.

We previously documented some of the mechanisms through which EES facilitates locomotion in rats. In particular, we showed that the modulation of reciprocal inhibitory circuits via proprioceptive feedback during each phase of gait directs the excitatory drive elicited by EES toward the motor neuron pools that are functionally relevant at that specific time[18]. This mechanism transforms the unspecific excitatory drive into a spatially and temporally specific pattern of excitation delivered alternatingly to the motor neuron pools whose activation is required in the flexion and extension phases of the step cycle. The spinal cord thus acts as an elegant filter that endows EES with the necessary specificity for therapeutic applications. Due to the cancellation of proprioceptive information in humans, only narrow ranges of EES frequencies and amplitudes can take advantage of this mechanism. Computer simulations indicate that EES disrupts movement-related modulation of reciprocal inhibitory circuits as soon as the stimulation elicits responses in muscles. The resulting destabilization of the network leads to an imbalance in the excitation of antagonist motor pools, favoring one motor pool over the other. Consequently, the modulation of EES parameters fails to enable the graded control over motor neuron activity that is observed in the rodent computational model. Experimental recordings confirmed these results, both in rodents and humans with SCI. We previously showed that this controllability enables targeting lesion-specific gait deficits and mediating task-specific adjustments of leg movements through closed-loop controllers and brain–spine interfaces in rats and nonhuman primates[3,5,18]. These features may be essential to facilitate the complex postural and propulsive requirements underlying the bipedal gait of humans.

Finally, input from proprioceptive organs plays a determinant role in steering the reorganization of residual descending pathways that helps restore locomotion after SCI. Genetically modified mice lacking functional proprioceptive circuits display defective rearrangements of descending projections after SCI, which abolish the extensive recovery occurring spontaneously in wild-type mice after the same injury[47]. Similarly, clinical studies reported that the preservation of proprioceptive information is a key predictor of recovery after neurotrauma[48], suggesting that this specific sensory channel may also contribute to steering the reorganization of residual neuronal pathways in humans. Therefore, the disruption of natural proprioception may reduce the ability of EES to augment neuroplasticity and recovery when delivered during rehabilitation. The multifaceted roles of proprioceptive information in coordinating locomotor functions and steering functional recovery after SCI emphasize the critical importance of identifying EES protocols that preserve proprioceptive information to fulfill the therapeutic potential of this treatment framework for clinical applications.

EES strategies that replace or preserve proprioceptive information. We exploited this new understanding to design sensory-compliant EES protocols that circumvent the cancellation of natural proprioception during EES. We first conceptualized a strategy that aims to replace the cancelled proprioceptive information with a spatiotemporal stimulation profile that encodes the natural firing rates of proprioceptive afferents from each muscle during locomotion. Computer simulations confirmed that this EES protocol not only preserves proprioceptive information but also augments the control over motor neuron activity, while preserving the alternation between antagonist muscles. Realistically, the afferents originating from a single muscle cannot be targeted specifically with current stimulation technologies. However, these stimulation protocols could be approximated with EES bursts delivered over spatially selective spinal cord regions, using a temporal sequence coinciding with the firing profile of the proprioceptive afferents innervating these specific spinal cord regions. This approach shares similarities with EES protocols that encode the spatiotemporal sequence of motor neuron activation during locomotion[27]. Compared to continuous EES, this targeted stimulation strategy enables a markedly higher degree of control over motor neuron activity in animal models of SCI[5,27]. The alternation of spatially selective bursts also preserves the natural proprioceptive information flowing in the dorsal roots that are not engaged by the stimulation. Our simulations suggest that the delivery of EES bursts should coincide with the profile of proprioceptive afferent firing, which can be partially out of phase with motor neuron activity. However, we believe that this protocol would enhance control over motor neuron activity and maximize the amount of preserved proprioceptive information. Such a stimulation strategy shares striking similarities with biomimetic approaches developed for the delivery of realistic tactile sensations in human amputees[49].

We found that the delivery of EES bursts with low amplitude but high frequency may be an alternative or complementary stimulation strategy to minimize the cancellation of proprioceptive information. Due to the low amplitude, the stimulation recruits a limited number of afferents. Each proprioceptive afferent synapses onto all the homonymous motoneurons[31,32]. Consequently, the repeated recruitment of these afferents by EES bursts at high frequency leads to a summation of EPSPs in motor neurons, which receive an overall amount of excitation equivalent to that induced by continuous EES at high amplitude and low frequency. However, all the nonrecruited afferents continue providing essential information about muscle length and tension changes. These results have general implications for EES protocols. First, modulating EES bursts allows them to augment the amount of excitation delivered to motor neurons without the need to increase the stimulation amplitude. Second, the lower amplitude requirements would improve the spatial selectivity of the stimulation, since the volume of the electrical field is proportional to the current amplitude.

These stimulation protocols require dedicated implantable pulse generators that allow delivery of EES bursts with high-frequency resolution through independent current sources that are controllable independently in real-time. Various companies are developing next-generation implantable pulse generators that partially meet these requirements. In parallel, we are conducting a clinical study using a commercially available stimulator that we upgraded to enable real-time control of spatially selective EES trains. We found that within 1 week, spatiotemporal stimulation enables independent weight-bearing locomotion in the three participants of the present study[50]. These combined findings stress the necessity of developing new neurotechnologies that support the implementation of strategies that preserve proprioception to facilitate motor control and steer plasticity with EES in humans.

Online content

Any methods, additional references, Nature Research reporting summaries, source data, statements of data availability and associated accession codes are available at https://doi.org/10.1038/s41593-018-0262-6.

Received: 5 June 2018; Accepted: 26 September 2018;
Published online: 31 October 2018

References

1. Kiehn, O. Decoding the organization of spinal circuits that control locomotion. *Nat. Rev. Neurosci.* **17**, 224–238 (2016).
2. van den Brand, R. et al. Restoring voluntary control of locomotion after paralyzing spinal cord injury. *Science* **336**, 1182–1185 (2012).
3. Wenger, N. et al. Closed-loop neuromodulation of spinal sensorimotor circuits controls refined locomotion after complete spinal cord injury. *Sci. Transl. Med.* **6**, 255ra133 (2014).
4. Musienko, P. et al. Somatosensory control of balance during locomotion in decerebrated cat. *J. Neurophysiol.* **107**, 2072–2082 (2012).
5. Capogrosso, M. et al. A brain-spine interface alleviating gait deficits after spinal cord injury in primates. *Nature* **539**, 284–288 (2016).
6. Asboth, L. et al. Cortico-reticulo-spinal circuit reorganization enables functional recovery after severe spinal cord contusion. *Nat. Neurosci.* **21**, 576–588 (2018).
7. Dimitrijevic, M. R., Gerasimenko, Y. & Pinter, M. M. Evidence for a spinal central pattern generator in humans. *Ann. NY Acad. Sci.* **860**, 360–376 (1998).
8. Minassian, K. et al. Stepping-like movements in humans with complete spinal cord injury induced by epidural stimulation of the lumbar cord: electromyographic study of compound muscle action potentials. *Spinal Cord* **42**, 401–416 (2004).
9. Herman, R., He, J., D'Luzansky, S., Willis, W. & Dilli, S. Spinal cord stimulation facilitates functional walking in a chronic, incomplete spinal cord injured. *Spinal Cord* **40**, 65–68 (2002).
10. Angeli, C. A. et al. Recovery of over-ground walking after chronic motor complete spinal cord Injury. *N. Engl. J. Med.* **379**, 1244–1250 (2018).
11. Gill, M. L. et al. Neuromodulation of lumbosacral spinal networks enables independent stepping after complete paraplegia. *Nat. Med.* **377**, 1938 (2018).
12. Harkema, S. et al. Effect of epidural stimulation of the lumbosacral spinal cord on voluntary movement, standing, and assisted stepping after motor complete paraplegia: a case study. *Lancet* **377**, 1938–1947 (2011).
13. Angeli, C. A., Edgerton, V. R., Gerasimenko, Y. P. & Harkema, S. J. Altering spinal cord excitability enables voluntary movements after chronic complete paralysis in humans. *Brain* **137**, 1394–1409 (2014).
14. Rattay, F., Minassian, K. & Dimitrijevic, M. R. Epidural electrical stimulation of posterior structures of the human lumbosacral cord: 2. quantitative analysis by computer modeling. *Spinal Cord* **38**, 473–489 (2000).
15. Capogrosso, M. et al. A computational model for epidural electrical stimulation of spinal sensorimotor circuits. *J. Neurosci.* **33**, 19326–19340 (2013).
16. Gerasimenko, Y. P. et al. Spinal cord reflexes induced by epidural spinal cord stimulation in normal awake rats. *J. Neurosci. Meth.* **157**, 253–263 (2006).
17. Minassian, K. et al. Human lumbar cord circuitries can be activated by extrinsic tonic input to generate locomotor-like activity. *Hum. Mov. Sci.* **26**, 275–295 (2007).
18. Moraud, E. M. et al. Mechanisms underlying the neuromodulation of spinal circuits for correcting gait and balance deficits after spinal cord injury. *Neuron* **89**, 814–828 (2016).
19. Su, C. F., Haghighi, S. S., Oro, J. J. & Gaines, R. W. "Backfiring" in spinal cord monitoring. High thoracic spinal cord stimulation evokes sciatic response by antidromic sensory pathway conduction, not motor tract conduction. *Spine* **17**, 504–508 (1992).
20. Hunter, J. P. & Ashby, P. Segmental effects of epidural spinal cord stimulation in humans. *J. Physiol. (Lond.)* **474**, 407–419 (1994).
21. Buonocore, M., Bonezzi, C. & Barolat, G. Neurophysiological evidence of antidromic activation of large myelinated fibres in lower limbs during spinal cord stimulation. *Spine* **33**, E90–E93 (2008).
22. Prochazka, A. Proprioceptive feedback and movement regulation. *Compr. Physiol.* **76**, 125 (1996).
23. Courtine, G. et al. Transformation of nonfunctional spinal circuits into functional states after the loss of brain input. *Nat. Neurosci.* **12**, 1333–1342 (2009).
24. Capaday, C. & Stein, R. B. Amplitude modulation of the soleus H-reflex in the human during walking and standing. *J. Neurosci.* **6**, 1308–1313 (1986).
25. Courtine, G., Harkema, S. J., Dy, C. J., Gerasimenko, Y. P. & Dyhre-Poulsen, P. Modulation of multisegmental monosynaptic responses in a variety of leg muscles during walking and running in humans. *J. Physiol. (Lond.)* **582**, 1125–1139 (2007).
26. Dy, C. J. et al. Phase-dependent modulation of percutaneously elicited multisegmental muscle responses after spinal cord injury. *J. Neurophysiol.* **103**, 2808–2820 (2010).
27. Wenger, N. et al. Spatiotemporal neuromodulation therapies engaging muscle synergies improve motor control after spinal cord injury. *Nat. Med.* **22**, 138–145 (2016).
28. Mignardot, J.-B. et al. A multidirectional gravity-assist algorithm that enhances locomotor control in patients with stroke or spinal cord injury. *Sci. Transl. Med.* **9**, eaah3621 (2017).
29. Conway, B. A., Hultborn, H. & Kiehn, O. Proprioceptive input resets central locomotor rhythm in the spinal cat. *Exp. Brain Res.* **68**, 643–656 (1987).
30. Prochazka, A. Quantifying proprioception. *Prog. Brain. Res.* **123**, 133–142 (1999).
31. Mendell, L. M. & Henneman, E. Terminals of single Ia fibers: location, density, and distribution within a pool of 300 homonymous motoneurons. *J. Neurophysiol.* **34**, 171–187 (1971).
32. Segev, I., Fleshman, J. W. Jr. & Burke, R. E. Computer simulation of group Ia EPSPs using morphologically realistic models of cat alpha-motoneurons. *J. Neurophysiol.* **64**, 648–660 (1990).
33. Collins, W. F. III, Honig, M. G. & Mendell, L. M. Heterogeneity of group Ia synapses on homonymous alpha-motoneurons as revealed by high-frequency stimulation of Ia afferent fibers. *J. Neurophysiol.* **52**, 980–993 (1984).
34. Koerber, H. R. & Mendell, L. M. Modulation of synaptic transmission at Ia-afferent connections on motoneurons during high-frequency afferent stimulation: dependence on motor task. *J. Neurophysiol.* **65**, 1313–1320 (1991).
35. Bawa, P. & Chalmers, G. Responses of human motoneurons to high-frequency stimulation of Ia afferents. *Muscle Nerve* **38**, 1604–1615 (2008).
36. Carhart, M. R., He, J., Herman, R., D'Luzansky, S. & Willis, W. T. Epidural spinal-cord stimulation facilitates recovery of functional walking following incomplete spinal-cord injury. *IEEE Trans. Neural Syst. Rehabil. Eng.* **12**, 32–42 (2004).
37. Proske, U. & Gandevia, S. C. The proprioceptive senses: their roles in signaling body shape, body position and movement, and muscle force. *Physiol. Rev.* **92**, 1651–1697 (2012).
38. Dietz, V. Proprioception and locomotor disorders. *Nat. Rev. Neurosci.* **3**, 781–790 (2002).
39. Tuthill, J. C. & Azim, E. Proprioception. *Curr. Biol.* **28**, R194–R203 (2018).
40. Sanes, J. N., Mauritz, K. H., Dalakas, M. C. & Evarts, E. V. Motor control in humans with large-fiber sensory neuropathy. *Hum. Neurobiol.* **4**, 101–114 (1985).
41. Cole, J. *Pride and a Daily Marathon* (MIT Press, Boston, MA, USA, 1995).
42. Dietz, V. & Duysens, J. Significance of load receptor input during locomotion: a review. *Gait Posture* **11**, 102–110 (2000).
43. Rossignol, S., Dubuc, R. & Gossard, J.-P. Dynamic sensorimotor interactions in locomotion. *Physiol. Rev.* **86**, 89–154 (2006).
44. Hultborn, H. & Nielsen, J. B. Spinal control of locomotion-from cat to man. *Acta Physiol. (Oxf.)* **189**, 111–121 (2007).
45. Prochazka, A. & Yakovenko, S. Predictive and reactive tuning of the locomotor CPG. *Integr. Comp. Biol.* **47**, 474–481 (2007).
46. Edgerton, V. R., Tillakaratne, N. J. K., Bigbee, A. J., de Leon, R. D. & Roy, R. R. Plasticity of the spinal neural circuitry after injury. *Annu. Rev. Neurosci.* **27**, 145–167 (2004).
47. Takeoka, A., Vollenweider, I., Courtine, G. & Arber, S. Muscle spindle feedback directs locomotor recovery and circuit reorganization after spinal cord injury. *Cell* **159**, 1626–1639 (2014).
48. Park, S.-W., Wolf, S. L., Blanton, S., Winstein, C. & Nichols-Larsen, D. S. The EXCITE Trial: predicting a clinically meaningful motor activity log outcome. *Neurorehabil. Neural. Repair.* **22**, 486–493 (2008).
49. Saal, H. P. & Bensmaia, S. J. Biomimetic approaches to bionic touch through a peripheral nerve interface. *Neuropsychologia* **79 Pt B**, 344–353 (2015).
50. Wagner, F. et al. Targeted neurotechnologies restore walking in humans with spinal cord injury. *Nature* https://doi.org/10.1038/s41593-018-0262-6 (2018).

Acknowledgements

We thank K. Bartholdi, A. Bichat, and L. Baud for their help with the rat experiments, and we thank all the individuals involved in the STIMO clinical study. This research was supported by the HBP Neurorobotics Platform, funded from the European Union's Horizon 2020 Framework Programme for Research and Innovation under the Specific Grant Agreement No. 720270 (Human Brain Project SGA1). Financial support was provided by the European Union's Horizon 2020 Framework Programme for Research and Innovation under Specific Grant Agreements No. 720270 (Human Brain Project SGA1) and No. 785907 (Human Brain Project SGA2); RESTORE: Eurostars E10889, Wings for Life, GTXmedical, Consolidator Grant from the European Research Council (ERC-2015-CoG HOW2WALKAGAIN 682999), Wyss Center for Neuroengineering, National Center of Competence in Research (NCCR) Robotics of the Swiss National Science Foundation, the Commission of Technology and Innovation (CTI) Innosuisse (CTI) OptiStim 25761.1, International Foundation for Research in Paraplegia (IRP), the Michel-Adrien Voirol Foundation, the Firmenich Foundation, the Pictet Group Charitable Foundation, the Panacée Foundation, and the Marie-Curie EPFL fellowship program.

Author contributions

E.F., M.C., K.M., S.M., and G.C. conceived the study. E.F. and M.C. designed the computational model and E.F. performed the simulations. J.B. performed the surgery in humans. E.F., K.M., F.W., J.B.M., and C.G.LG. performed the experiments. A.R. and E.F. built the robotic platform to control rat ankle kinematics. E.F. performed the

data analyses and prepared the figures. G.C. wrote the manuscript with E.F., M.C., and K.M., and all the authors contributed to its editing. G.C., S.M., M.C., and J.B. supervised the work.

Competing interests

G.C, J.B., and S.M. are founders and shareholders of GTXmedical SA, a company developing neuroprosthetic systems in direct relationship with the present work. E.F., M.C., G.C., and S.M. hold several patents related to electrical spinal cord stimulation.

Additional information

Supplementary information is available for this paper at https://doi.org/10.1038/s41593-018-0262-6.

Reprints and permissions information is available at www.nature.com/reprints.

Correspondence and requests for materials should be addressed to G.C.

Publisher's note: Springer Nature remains neutral with regard to jurisdictional claims in published maps and institutional affiliations.

Methods

Computer simulations. Computer simulations were performed in Python 2.7 using the NEURON[51] simulation environment to run the spiking neural network models and OpenSim[52] for the biomechanical model of rats and humans. Both the NEURON simulation environment and OpenSim are open-source programs.

Model of a proprioceptive afferent fiber recruited by EES. The afferent fiber model was characterized by two parameters: (i) the propagation time required by an AP to travel the whole length of the fiber, and (ii) the firing rate at which APs are generated by the sensory organ. These parameters were adjusted to meet the properties of all the modeled afferent fibers. For each AP, we simulated the propagation from the sensory organ of origin to the spinal cord and the refractory dynamics (mean refractory period ± s.d.: 1.6 ± 0.16 ms) along the fiber. We modeled EES as a periodic event recruiting the most proximal portion of the fiber. The recruitment only occurred when the fiber was not in its refractory period. When a fiber was electrically activated, an antidromic AP propagated toward the distal end of the fiber. The encounter of this antidromic AP with a sensory AP traveling toward the spinal cord led to an antidromic collision that cancelled both APs.

Estimation of antidromic collisions probability. The developed fiber model was used to assess the probability of antidromic collisions based on EES frequency, the firing rate of the sensory organs, and the propagation time required for an AP to travel along the whole length of the fiber. Propagation times were set to 2 ms in rat afferents. Due to the extended length of axons in humans, we modeled human afferents innervating proximal (10 ms) and distal (20 ms) muscles. Antidromic collision probability was defined as the probability of a natural sensory AP to collide with an EES-induced antidromic AP within a single fiber. For each tested model parameter and stimulation frequency, we integrated the dynamic of the fiber over 60 s and evaluated the number of antidromic collisions occurring within this time period. To estimate the antidromic collision probability, we averaged the results of 50 simulations initialized with different EES onset delays varying between 0 and 10 ms.

Rat model of proprioceptive feedback circuits. The rat model of proprioceptive feedback circuits was elaborated from a previously validated model[18], which we modified to integrate a simpler and faster model of the motor neurons with the new model of proprioceptive afferents that considers the occurrence of antidromic collisions.

Briefly, this model is composed of four components: (i) a spiking neural network reproducing the proprioceptive feedback circuits associated with a pair of antagonist muscles, (ii) a muscle spindle model, (iii) a musculoskeletal model of the rat hindlimb, and (iv) a finite-element method model of EES of the rat lumbar spinal cord (Fig. 4a).

The spiking neural network includes populations of group-Ia and group-II afferent fibers, Ia-inhibitory interneurons, group-II excitatory interneurons, and pools of alpha motor neurons. The number of cells, the number and the strength of the synapses contacting the different populations of neurons, and the characteristics of the cell models are described in our previous work[18]. To speed up the simulation time, we replaced our previous multicompartmental motor neuron model with an integrate-and-fire cell model designed to reproduce realistic membrane response dynamics to excitatory and inhibitory stimuli[53–56]. Specifically, we set the refractory period to 20 ± 1 ms and the membrane time constant $\tau_{membrane}$ to 6 ± 0.3 ms. Excitatory synapses were modeled as instantaneous changes in current, exponentially decaying with time constant $\tau_{excitatory} = 0.25$ ms. Inhibitory synapses were modeled as alpha functions with a rise time constant $\tau_{inhibitory\_1} =$ 2 ms and a decay time constant $\tau_{inhibitory\_2} = 4.5$ ms (Supplementary Fig. 7a). We adjusted the motor neurons synaptic weights to match experimental excitatory and inhibitory postsynaptic potentials (EPSPs/IPSPs). For this, we normalized experimental EPSPs[54,55] and IPSPs[56] to the minimum depolarization necessary to induce an AP in our multicompartmental model (Supplementary Fig. 7b,c). Afferent fibers were modeled with an AP propagation time of 2 ms. This parameter was estimated to represent rat afferent fibers innervating the antagonist muscles of the ankle.

Musculoskeletal[57,58] and muscle spindle[30] models were used to calculate the firing rate profiles of group-Ia and group-II afferent fibers innervating the flexor (tibialis anterior) and extensor (gastrocnemius medialis) muscles of the ankle during locomotion. For this purpose, we steered the musculoskeletal model with previously obtained recordings of rat hindlimb kinematics during locomotion to estimate the ankle muscles stretch profiles through inverse kinematics. We then used the muscle spindle model to compute the firing rate profiles. To mimic the alpha–gamma linkage, muscle stretch and stretch velocity were linked to the envelope of EMG activity from the homonymous muscle (equations (1) and (2)[30]). The estimated afferent firing rate profiles drove the activity of the modeled proprioceptive afferents.

A validated finite element model of EES of the lumbar spinal cord[15] was finally used to estimate the proportion of afferent and efferent fibers recruited at a given stimulation amplitude. Realistic interactions between EES and the natural sensory activity along the modeled afferent fibers were integrated using the developed proprioceptive afferent model.

$$\text{Ia firing rate} = 50 + 2 \cdot stretch + 4.3 \cdot sign(stretchVelocity) \cdot |stretchVelocity|^{0.6} + 50 \cdot EMG_{env} \quad (1)$$

$$\text{II firing rate} = 80 + 13.5 \cdot stretch + 20 \cdot EMG_{env} \quad (2)$$

Human model of proprioceptive feedback circuits. The layout of the rat model served as a basis to build the human model of proprioceptive feedback circuits. To take into account the specific anatomical and physiological features of humans, we adapted the musculoskeletal model, the muscle spindle model, the weights of the synapses in the network, the length of the modeled afferent fibers, and the output of the finite element method model of EES (Fig. 4a).

To estimate the stretch of flexor (tibialis anterior) and extensor (soleus) muscles spanning the ankle joints, we used the 3DGaitModel2392 OpenSim lower limb model[59] and kinematic data from healthy subjects during locomotion on a treadmill[28,60]. We tuned the muscle spindle model to account for the lower firing rates of human proprioceptive afferents compared to those of rodents[22,61]. Specifically, we scaled equations (1) and (2) down by 0.2 and 0.25, respectively, to produce firing rates that remained within the range of values generally observed in humans (rarely exceeding 30 impulses/s[22,30,62]). Envelopes of EMG activity were extracted from the same subjects from whom we also extracted the kinematic data[28,60].

We assumed that if the occurrence probabilities of antidromic collisions were the same in humans and rodents, the human model should reproduce results qualitatively similar to the simulations obtained in rats. Hence we optimized the weight of the synaptic connections between the afferent fibers and their target spinal neurons by driving the network with the estimated human afferent firings but without modifying the propagation time required by sensory APs to reach the spinal cord, a parameter proportional to the occurrence probability of antidromic collisions (Supplementary Fig. 8a). To this purpose we performed a systematic search by progressively increasing the synaptic weights of connections from afferent fibers. EES frequency and percentage of Ia afferents recruited by EES were set to 60 Hz and to 60%, respectively. We defined a set of fitness functions and relative minimum scores to define the range of synaptic weights that produce the desired behavior of the network (equation (3)) and selected one set of weights for further simulations (Supplementary Fig. 8b,c).

$$\begin{Bmatrix} percentile\_90(\boldsymbol{MotoneuronsFR_{ext}}) > 5 \text{ Imp/s} \\ percentile\_90(\boldsymbol{MotoneuronsFR_{flex}}) > 5 \text{ Imp/s} \\ 1 - mean(\boldsymbol{MotoneuronsFR_{ext}} \cdot \boldsymbol{MotoneuronsFR_{flex}}) > 9 \end{Bmatrix} \quad (3)$$

We then modified the AP propagation-time parameter of the afferent fiber models to 16 ms, which is a representative value for the proprioceptive afferents of the ankle muscles in humans[63].

We assumed that the ratio of the amount of primary vs. secondary afferent fibers recruited by EES while increasing the stimulation amplitude would be similar in rats and humans. We thus used the finite-element model of the rat spinal cord to estimate the percentage of primary and secondary afferents recruited by the stimulation. However, to account for the considerably larger distance of the ventral roots from the epidural electrodes, we did not simulate the direct recruitment of motor axons. This phenomenon commonly occurs in rats but is limited in humans[14,15]. While this decision was taken in order to build a more realistic model, simulating the direct recruitment of motor axons as in the rat model would have not influenced the significance of the presented results. Indeed, given the low amplitudes tested in this work, only 7% of the simulated rat motor neuron axons were recruited directly by EES at the highest stimulation amplitude tested (Fig. 5a).

Spatiotemporal stimulation profiles. Spatiotemporal EES profiles encoding the natural proprioceptive information originating from a pair of antagonist muscles spanning the ankle joint were estimated in two steps. First, we computed the normalized average firing rate profiles of group-Ia, group-II, and group-Ib afferents over a gait cycle. Second, these three profiles were averaged to produce a stimulation profile that encodes the global proprioceptive information (Fig. 7a). Since group-Ib afferent firing is closely correlated to the activity of the muscle along which the associated Golgi tendon organ is connected[30], we approximated the firing rates of group-Ib afferents with the envelope of the EMG activity from the homonymous muscle during gait. Simulations were conducted using the estimated stimulation profile for each muscle. EES amplitude was adjusted proportionally to the changes in the estimated stimulation profile, while the length of the stimulation profile was adjusted based on the duration of each gait cycle.

High-frequency, low-amplitude EES model. To assess the effect of high-frequency, low-amplitude EES on the membrane potentials of motor neurons, we used our previously validated multicompartmental motor neuron model, which

integrates realistic synaptic boutons from group-Ia afferents[18] (Fig. 8a,b). However, simulations on the effect of high-frequency low-amplitude EES on the muscle spindle feedback circuits were performed using the simplified integrate-and-fire motor neuron model (Supplementary Fig. 7). The more realistic multicompartmental model was used in order to obtain a more accurate estimate of motor neurons' soma responses to high-frequency bursts of EES.

Limitations of the human computational model. Microneurographic recordings of group-Ia and group-II afferents during slow movements reported that firing rates rarely exceed 30 Imp/s in humans[22,64,65]. In the human computational model, we thus limited muscle spindle firing to 50 Imp/s during gait, which is markedly lower than peak firings of up to 200 Imp/s reported during locomotion in quadrupedal mammals. Nevertheless, we cannot exclude the possibility that human muscle spindle afferents fire at higher rates during gait. Indeed, locomotion involves higher movement speeds than those commonly used during microneurographic recordings in humans. Consequently, the actual range of firing rates underlying the activity of group-Ia fibers during human gait remains unknown. While higher firing rates might affect the predictions of our model, the overall conclusions would remain unchanged, since EES would still block a substantial amount of proprioceptive information for high firing rates. Therefore, the degree of disruption may scale with the actual range of afferent firings, but the conclusion derived from this model would still hold.

Experimental procedures in humans. *Spinal cord stimulation system implanted in human subjects with SCI.* Experiments conducted in human subjects with SCI were carried out within the framework of an ongoing clinical study (ClinicalTrials.gov identifier: NCT02936453) which has been approved by Swiss authorities (Swissethics protocol number 04/2014 project ID: PB_2016-00886, Swissmedic protocol 2016-MD-0002), and were in compliance with all relevant clinical regulations. The study is conducted at the Lausanne University Hospital (CHUV). All subjects gave written informed consent before their participation. Subjects were surgically implanted with a spinal cord stimulation system comprising an implantable pulse generator (Activa RC, Medtronic Plc., Fridley, Minnesota, SA) connected to a 16-electrode paddle array (Medtronic Specify 5-6-5 surgical lead) that was placed over the lumbosacral segments of the spinal cord. Subject-related data and details on their neurological status at their entry into the clinical study, evaluated according to the International Standards for Neurological Classification of Spinal Cord Injury, are provided in the Nature Research Reporting Summary and in Supplementary Table 1. The subject-recruitment process is described in the Nature Research Reporting Summary.

Recording of EES-induced antidromic activity along human afferents. Recordings of the neural activity induced by EES were performed with the NIM Eclipse system (Medtronic Plc., Fridley, Minnesota, USA). The activity of the soleus muscle was recorded with surface EMG electrodes (Ambu Neuroline 715, Ambu Sarl, Bordeaux, France), while the activity of the sural and of the proximal and distal branches of the tibial nerve were recorded using percutaneous disposable needle electrodes (Ambu Neuroline Twisted Pair Subdermal 12 × 0.4 mm, Ambu Sarl, Bordeaux, France). The proximal branch of the tibial nerve was recorded at the level of the popliteal fossa (Fig. 2a). The recording needle electrode was inserted at the site that elicited an H-reflex at the lowest stimulation amplitude, identified using a stimulation probe. The distal branch of the tibial nerve was recorded at the level of the medial malleolus (Fig. 2a). The recording electrode position was determined by applying electrical stimulation to this site and by verifying the evoked potentials at the level of the proximal branch of the tibial nerve. The sural nerve was recorded at the level of the lateral malleolus. The specific location of the electrode was defined following the same procedure used for the distal branch of the tibial nerve. Neural and EMG signals were sampled at 10,000 Hz, amplified, and bandpass-filtered (30–1,000 Hz) online. For the entire duration of the experiment, participants remained relaxed in a supine position. EES was delivered at 20 Hz for 60 s to collect a total of approximately 1,200 pulses. We selected EES sites that mainly recruited the posterior root innervating the S1 spinal segment, as verified in the presence of reflex responses in the soleus muscle following each pulse of EES. For the experiment, the stimulation amplitude was reduced until no muscle contraction was noticeable, to avoid contaminating neural recordings with electromyographic activity or movement artifacts. To verify that the stimulation amplitude was sufficient to recruit afferent fibers in the recorded nerves, we confirmed that the stimulation elicited a sensation of tingling in the corresponding dermatome. We recorded EES artifacts with surface electrodes positioned over the vertebral levels of the implanted paddle array. The artifacts were used as triggers to extract and average the evoked potentials.

Assessment of proprioceptive function during EES. The threshold to detection of passive movement test[66] was performed with the Humac Norm Cybex system (Computer Sports Medicine Inc., Stoughton, US). Subjects were first tested without EES and then during continuous EES. Throughout the experiment, participants' tactile, visual, and aural information were occluded using foam cushions, blindfolds, and headphones with pink noise. The experimental protocol was tailored for each participant, since each of them presented distinct levels of residual proprioceptive functions. At the beginning of each trial, the participant's knee joint was moved to an initial position of 45° of extension. The participant was informed with a tap on the shoulder that a new trial was about to start. The trial was then started after a randomized time delay to assess false positive detections. In subject #1, we imposed movements of knee extension or knee flexion from the initial position at a constant angular velocity of 0.5° s^{-1}. Flexion and extension were delivered randomly. The participant was instructed to report the movement direction, as soon as he became aware of it, by pushing a button. A maximum displacement of 15° was allowed (Fig. 2b). Button-triggered digital signals and joint kinematics were recorded at a sampling frequency of 5,000 Hz. The trial was considered successful if the direction of the movement was correctly identified. A trial was considered unsuccessful when the movement was either misclassified or not perceived at all within the limited range of movement. Subject #3 was not able to detect the direction of the imposed movement, even in the absence of continuous EES. To simplify the task, we limited the movement to knee extension only, increased the movement speed to 1° s^{-1}, and allowed a maximum displacement of 30° (Fig. 2b). A trial was considered successful if the movement was detected within the allowed range of movement. Subject #2 was not able to perceive the imposed movements and was thus excluded from this experiment.

A minimum of 10 repetitions were performed to complete an assessment for a given EES condition. The ratio of successful and unsuccessful trials was used to compute participants' error rate and 95% confidence interval using the Clopper–Pearson interval method based on a beta distribution.

We adjusted the configuration of EES electrodes to target both flexor and extensor muscles of the knee. Recordings of EMG activity from the vastus lateralis and semitendinosus muscles allowed us to identify the minimum stimulation amplitude necessary to recruit these muscles. We then assessed the proprioceptive functions of the subjects during continuous EES that was delivered with amplitudes below (0.8×) and above (1.5×) the muscle response threshold. For both amplitudes, we tested a range of frequencies: 10, 30, 50, and 100 Hz. At 1.5× the muscle response threshold amplitude, frequencies below 50 Hz induced spastic contractions and were thus not further tested. The sequence of the tested stimulation parameters was randomized.

Assessment of EES-induced responses modulated during passive joint movements. The Humac Norm Cybex was used to impose passive joint movements with a sinusoidal profile of fixed amplitude and frequency, while continuous EES was delivered to produce motor responses in the muscles spanning this joint. The subjects were asked to relax and not to resist, follow, or facilitate the movements. Muscle responses and EES artifacts were recorded with wireless surface EMG electrodes (Myon 320, Myon AG, Schwarzenberg, Switzerland) at a sampling frequency of 5,000 Hz. Joint kinematics was recorded with the Cybex system at 5,000 Hz. EES parameters, as well as the targeted joint, angular velocity, and amplitude of the movement, were set depending on subject-specific constraints (Fig. 3a and Supplementary Fig. 2). In subject #1, the Cybex system was used to produce flexion and extension movements of the ankle joint at a frequency of 1.13 Hz and a range of motion of 30°. These parameters were chosen to be as large as possible in order to maximize the amount of proprioceptive signals generated from the targeted muscles while minimizing discomfort. EES electrodes were configured to recruit the targeted muscles. EES was delivered with frequencies ranging from 5 to 60 Hz, presented in a random order. The stimulation amplitude was set to induce consistent muscle responses across the range of tested frequencies, corresponded to 1.25× the muscle response threshold. For each condition tested, a minimum of 1 min of recording was performed. Recording duration was extended to 2 min when EES was delivered at 5 Hz. In subjects #2 and #3, we could not find electrode configurations that recruited the targeted muscles without causing discomfort at the required EES amplitudes and frequencies. Therefore, we adapted the experiment and targeted the knee joint instead of the ankle joint. Moreover, we limited the range of tested frequencies. Specifically, for subject #3 we kept an oscillation frequency of 1.13 Hz, set a movement range of 60°, and limited the range of EES frequencies from 10 to 60 Hz. These settings also led to spastic contractions in subject #2. Consequently, we reduced the movement range and frequency to 50° and 0.9 Hz, respectively, and limited the range of EES frequencies between 20 and 60 Hz.

To quantify the modulation of muscle responses during the passive movements, we extracted the timing of each EES pulse with the recorded stimulation artifacts. We then extracted the muscles responses and grouped them according to the phase of the cyclic movement ($n = 10$ bins; Fig. 3b). When more than one EES pulse occurred within a given bin, only the response with highest amplitude was selected. We bootstrapped the normalized modulation depth median and 95% confidence interval (equation (4)) by computing the median peak-to-peak amplitudes (*mP2P*) of the responses in the different bins. Normalization was performed to account for frequency-dependent depression of EES-induced muscle responses[67–69].

$$NormalizedModulationDepth = \frac{[\max(mP2Ps) - \min(mP2Ps)]}{\min(mP2Ps)} \quad (4)$$

Continuous EES during locomotion on a treadmill. The FLOAT robotic suspension system (Lutz Medical Engineering AG, Rudlingen, Switzerland) was used to provide the participants with personalized upward and forward forces to the trunk during locomotion on a treadmill[28,70]. EES was delivered through four independent configurations of electrodes. Each configuration involved one or multiple anodes and cathodes. We configured these electrode combinations to target the left and right posterior roots projecting to the L1 and L4 segments. For this purpose, we searched the electrode configurations that activated preferentially the iliopsoas and the tibialis anterior. These motor pools spanned the L1/L2 segments and L4/L5 segments, respectively. The amplitudes and frequencies of these four electrode configurations were optimized by visual inspection of the induced EMG activity and facilitation of kinematics when subjects were asked to step on the treadmill. Different EES frequencies and amplitudes were tested to characterize the ability of EES to modulate the motor output. The order of the tested parameters was randomized. EMG recordings were performed with wireless surface electrodes (Myon 320, Myon AG, Schwarzenberg, Switzerland) and recorded at 1,000 Hz. Leg kinematics was recorded using the Vicon motion capture system (Vicon Motion Systems, Oxford, UK) at 100 Hz. Subjects were allowed to use the handrails of the treadmill to facilitate their leg movements. Analysis of EMG activity and kinematics were conducted using methods reported in detail previously[28].

Electrophysiological recordings of high-frequency, low-amplitude EES. EES was delivered through electrode configurations used to facilitate locomotion. Motor responses to both single pulses and bursts of 4 pulses at 500 Hz were recorded from different lower limb muscles with wireless surface electrodes at a sampling rate of 5,000 Hz (Myon 320, Myon AG, Schwarzenberg, Switzerland). The responses of the most-recruited muscle were used for analyses. During the experiment, the participants were in the supine position.

Experimental procedures in rats. *Animal husbandry.* All procedures and surgeries were approved by the Veterinary Office of the canton of Geneva in Switzerland, and were in compliance with all relevant ethical regulations. The experiments were conducted in nine 11-week-old female Lewis rats (~220-g body weight) and four 11-week-old Long-Evans rats (~240-g body weight). Rats were housed separately on a light/dark cycle of 12 h.

Surgical procedures. Surgical procedures have been described in detail previously[2,23]. All interventions were performed in aseptic conditions and under general anesthesia. Briefly, rats received a severe thoracic (T8) contusion SCI (250 kdyn) inflicted by a force-controlled spinal cord impactor (IH-0400 Impactor, Precision Systems and Instrumentation LLC, USA). During the same surgery, EES electrodes were sutured to the dura overlying the midline of S1 and L2 spinal segments in Lewis rats and of L4 and L2 spinal segments in Long-Evans rats. Electrodes were created by removing a short length of insulation (~400 µm) from Teflon-coated stainless-steel wires (AS632, Cooner Wire, USA). A common ground wire electrode (~1 cm of active site) was placed subcutaneously over the right shoulder. Finally, bipolar electrodes (same type as used for EES) were implanted bilaterally in the left and right tibialis anterior muscles to record the EMG activity.

Assessment of EES-induced responses modulated during passive joint movements. Lewis rats ($n = 4$) were lightly anesthetized (ketamine: 75 mg/kg and xylazine 5 mg/kg, i.p.) and positioned in a prone position within a support system that let the hindlimbs hanging freely. The right paw was secured within a 3D-printed pedal connected to a stepper motor (QSH4218-51-10-049, Trinamic Motion Control GmbH, Waterloohain, Germany). We used this robotic platform to impose cyclic movements of the ankle with a fixed amplitude (70°) and frequency (0.54 Hz), while continuous EES was delivered to evoke responses in the tibialis anterior muscle (Fig. 3e). EES was delivered using an IZ2H Stimulator controlled by a RZ2 BioAmp Processor (Tucker-Davis Technologies, Alachua, US). EES amplitude was set to approximately 1.2× the muscle response threshold. We tested EES frequencies ranging from 5 to 100 Hz, delivered in a random order. EMG activity of the tibialis anterior was amplified with a PZ3 Low Impedance Amplifier (Tucker-Davis Technologies, Alachua, US) and recorded with the RZ2 BioAmp Processor at a sampling frequency of 24,414 Hz. Ankle kinematics was record with the Vicon motion capture system at a sampling frequency of 200 Hz. For each tested EES condition, a minimum of 1 min of recording was performed. To analyze the modulation of the muscle responses, we used the same procedures that we adopted in the equivalent experiment carried out in human subjects.

Electrophysiological recordings of high-frequency, low-amplitude EES. We tested the impact of high-frequency, low-amplitude EES in $n = 5$ Lewis rats. EES and EMG recordings were performed with the setup used for assessing the modulation of muscle responses during passive movements. The muscle response threshold was measured using single pulses of EES that were delivered at amplitudes close to this threshold, thus allowing us to obtain a precise value. High-frequency bursts were then delivered at amplitudes below the identified motor response threshold. The aim was to evaluate whether high-frequency stimulation was able to recruit motor neurons trans-synaptically at lower amplitudes than single pulses. For each amplitude, we tested burst frequencies ranging from 100 to 1,000 Hz. The duration of each burst was kept constant at 25 ms. During the experiments, the rats were held in a resting position with the hindlimbs hanging freely.

Continuous EES during locomotion on a treadmill. Behavioral experiments during locomotion were performed in $n = 4$ Long-Evans rats. Following 1–2 weeks of rehabilitation using previously described procedures[2,23], we evaluated the impact of different EES frequencies on the modulation of muscle activity and hindlimb kinematics during bipedal locomotion on a treadmill. Locomotion was recorded without EES and with EES at frequencies ranging from 20 to 80 Hz, delivered in a random order. EES amplitude was kept fixed at the optimal value found during training. For each experimental condition, approximately 10 gait cycles or 20 s of minimal leg movements were recorded.

Hindlimb kinematics was recorded with the Vicon motion capture system (Vicon Motion Systems, Oxford, UK) at a sampling frequency of 200 Hz. EMG signals were amplified and filtered online (10- to 10,000-Hz bandpass filter) by a Differential AC Amplifier (A-M System, Sequim, US) and recorded at 2,000 kHz with the Vicon system.

Statistics. No statistical methods were used to predetermine sample sizes, but our sample sizes are similar to those reported in previous publications using similar experimental procedures[13,15,18,66]. Data collection and analysis were not performed blind to the conditions of the experiments. No data were excluded from the analyses. Different EES conditions were tested on the same animals or participants, and thus no control groups were used. In each experiment, the order of the tested EES conditions was randomized as described in the relevant Methods sections and in the Nature Research Reporting Summary. Data are reported as mean ± s.e.m. or median values ± 95% confidence interval (CI). Confidence intervals and significance were analyzed using nonparametric two-sided Wilcoxon rank-sum tests with Bonferroni correction for multiple comparisons, two-tailed Wald tests, the Clopper–Pearson interval based on a beta distribution, or a bootstrapping approach based on the Monte Carlo algorithm resampling scheme ($n = 10{,}000$ iterations). Linear regression between step height and EES frequency (Fig. 6c) was performed assuming a normal distribution of the residuals around zero, but normality was not formally tested for. We made no other assumptions.

Reporting Summary. Further information on research design is available in the Nature Research Reporting Summary linked to this article.

Code availability. Software routines developed for data analysis are available from the corresponding author upon reasonable request. The code for performing and analyzing the neural simulations is available as Supplementary Software and at https://github.com/FormentoEmanuele/MuscleSpindleCircuitsModel.git.

Data availability

Acquired data are available from the corresponding author upon reasonable request.

References

51. Hines, M. L. & Carnevale, N. T. The NEURON simulation environment. *Neural Comput.* **9**, 1179–1209 (1997).
52. Delp, S. L. et al. OpenSim: open-source software to create and analyze dynamic simulations of movement. *IEEE Trans. Biomed. Eng.* **54**, 1940–1950 (2007).
53. Burke, R. E. Group Ia synaptic input to fast and slow twitch motor units of cat triceps surae. *J. Physiol. (Lond.)* **196**, 605–630 (1968).
54. Munson, J. B., Fleshman, J. W. & Sypert, G. W. Properties of single-fiber spindle group II EPSPs in triceps surae motoneurons. *J. Neurophysiol.* **44**, 713–725 (1980).
55. Harrison, P. J. & Taylor, A. Individual excitatory post-synaptic potentials due to muscle spindle Ia afferents in cat triceps surae motoneurones. *J. Physiol. (Lond.)* **312**, 455–470 (1981).
56. McIntyre, C. C. & Grill, W. M. Extracellular stimulation of central neurons: influence of stimulus waveform and frequency on neuronal output. *J. Neurophysiol.* **88**, 1592–1604 (2002).
57. Johnson, W. L., Jindrich, D. L., Roy, R. R. & Reggie Edgerton, V. A three-dimensional model of the rat hindlimb: musculoskeletal geometry and muscle moment arms. *J. Biomech.* **41**, 610–619 (2008).
58. Johnson, W. L., Jindrich, D. L., Zhong, H., Roy, R. R. & Edgerton, V. R. Application of a rat hindlimb model: a prediction of force spaces reachable through stimulation of nerve fascicles. *IEEE Trans. Biomed. Eng.* **58**, 3328–3338 (2011).
59. Delp, S. L. et al. An interactive graphics-based model of the lower extremity to study orthopaedic surgical procedures. *IEEE Trans. Biomed. Eng.* **37**, 757–767 (1990).
60. Wojtusch, J. & von Stryk, O. HuMoD - A versatile and open database for the investigation, modeling and simulation of human motion dynamics on actuation level. *IEEE-RAS International Conference on Humanoid Robots (Humanoids)* **15**, 74–79 (2015).

61. Hník, P. & Lessler, M. J. Changes in muscle spindle activity of the chronically de-efferented gastrocnemius of the rat. *Pflugers Arch.* **341**, 155–170 (1973).
62. Albert, F., Bergenheim, M., Ribot-Ciscar, E. & Roll, J.-P. The Ia afferent feedback of a given movement evokes the illusion of the same movement when returned to the subject via muscle tendon vibration. *Exp. Brain Res.* **172**, 163–174 (2006).
63. Restuccia, D. et al. Somatosensory evoked potentials after multisegmental lower limb stimulation in focal lesions of the lumbosacral spinal cord. *J. Neurol. Neurosurg. Psychiatry* **69**, 91–95 (2000).
64. Vallbo, A. B. & al-Falahe, N. A. Human muscle spindle response in a motor learning task. *J. Physiol. (Lond.)* **421**, 553–568 (1990).
65. Roll, J.-P., Albert, F., Ribot-Ciscar, E. & Bergenheim, M. "Proprioceptive signature" of cursive writing in humans: a multi-population coding. *Exp. Brain Res.* **157**, 359–368 (2004).
66. Han, J., Waddington, G., Adams, R., Anson, J. & Liu, Y. Assessing proprioception: A critical review of methods. *J. Sport Health Sci.* **5**, 80–90 (2016).
67. Ishikawa, K., Ott, K., Porter, R. W. & Stuart, D. Low frequency depression of the H wave in normal and spinal man. *Exp. Neurol.* **15**, 140–156 (1966).
68. Calancie, B. et al. Evidence that alterations in presynaptic inhibition contribute to segmental hypo- and hyperexcitability after spinal cord injury in man. *Electroencephalogr. Clin. Neurophysiol.* **89**, 177–186 (1993).
69. Schindler-Ivens, S. & Shields, R. K. Low frequency depression of H-reflexes in humans with acute and chronic spinal-cord injury. *Exp. Brain Res.* **133**, 233–241 (2000).
70. Vallery, H. et al. Multidirectional transparent support for overground gait training. *IEEE Int. Conf. Rehabil. Robot.* **2013**, 6650512–6650517 (2013).

nature research

Corresponding author(s): Gregoire Courtine: NN-A64473B

Reporting Summary

Nature Research wishes to improve the reproducibility of the work that we publish. This form provides structure for consistency and transparency in reporting. For further information on Nature Research policies, see Authors & Referees and the Editorial Policy Checklist.

Statistical parameters

When statistical analyses are reported, confirm that the following items are present in the relevant location (e.g. figure legend, table legend, main text, or Methods section).

n/a	Confirmed	
☐	☒	The exact sample size (*n*) for each experimental group/condition, given as a discrete number and unit of measurement
☐	☒	An indication of whether measurements were taken from distinct samples or whether the same sample was measured repeatedly
☐	☒	The statistical test(s) used AND whether they are one- or two-sided *Only common tests should be described solely by name; describe more complex techniques in the Methods section.*
☐	☒	A description of all covariates tested
☐	☒	A description of any assumptions or corrections, such as tests of normality and adjustment for multiple comparisons
☐	☒	A full description of the statistics including central tendency (e.g. means) or other basic estimates (e.g. regression coefficient) AND variation (e.g. standard deviation) or associated estimates of uncertainty (e.g. confidence intervals)
☐	☒	For null hypothesis testing, the test statistic (e.g. *F*, *t*, *r*) with confidence intervals, effect sizes, degrees of freedom and *P* value noted *Give P values as exact values whenever suitable.*
☒	☐	For Bayesian analysis, information on the choice of priors and Markov chain Monte Carlo settings
☒	☐	For hierarchical and complex designs, identification of the appropriate level for tests and full reporting of outcomes
☐	☒	Estimates of effect sizes (e.g. Cohen's *d*, Pearson's *r*), indicating how they were calculated
☐	☒	Clearly defined error bars *State explicitly what error bars represent (e.g. SD, SE, CI)*

Our web collection on statistics for biologists may be useful.

Software and code

Policy information about availability of computer code

Data collection	Data collection was performed with the following commercial and custom code: - NIM Eclipse system software (Medtronic plc, Fridley, Minnesota, USA), to record the neural activity induced by epidural electrical stimulation (EES) in humans. - Custom code developed using the TwinCat software system (Beckhoff Automation GmbH & Co. KG, Verl, Germany), to record joint kinematic and surface EMG signals during the assessment of proprioceptive functions, and during the assessment of EES-induced responses during passive joint movements performed in humans. - The Vicon motion capture system software (Vicon Motion Systems, Oxford, UK), to record kinematic and EMG signals during treadmill locomotion in rats and humans, and to record the ankle kinematic during the assessment of EES-induced responses during passive joint movements performed in rats. - Custom code developed in RPvdsEx to control an RZ2 BioAmp Processor (Tucker-Davis Technologies, Alachua, US), to record EMG signals in rats.
Data analysis	Computer simulations were performed in python 2.7 using the NEURON simulation environment to run the spiking neural network models and OpenSim for the biomechanical model of rats and humans. The code to perform and analyze the neural simulations is available as supplementary information and at https://github.com/FormentoEmanuele/MuscleSpindleCircuitsModel.git. Custom python 2.7 code was developed for data analyses, using the SciPy and StatsModels modules for statistical tests.

For manuscripts utilizing custom algorithms or software that are central to the research but not yet described in published literature, software must be made available to editors/reviewers upon request. We strongly encourage code deposition in a community repository (e.g. GitHub). See the Nature Research guidelines for submitting code & software for further information.

Data

Policy information about availability of data

All manuscripts must include a data availability statement. This statement should provide the following information, where applicable:

- Accession codes, unique identifiers, or web links for publicly available datasets
- A list of figures that have associated raw data
- A description of any restrictions on data availability

Acquired data are available from the corresponding author upon reasonable request.

Field-specific reporting

Please select the best fit for your research. If you are not sure, read the appropriate sections before making your selection.

☒ Life sciences ☐ Behavioural & social sciences ☐ Ecological, evolutionary & environmental sciences

For a reference copy of the document with all sections, see nature.com/authors/policies/ReportingSummary-flat.pdf

Life sciences study design

All studies must disclose on these points even when the disclosure is negative.

Sample size	No statistical methods were used to pre-determine sample sizes but our sample sizes are similar to those reported in previous publications using similar experimental procedures.
Data exclusions	No data were excluded from the analyses.
Replication	All experimental findings were replicated different times. For example, experiments in humans and rats during walking were collected multiple times on different days with the same outcomes
Randomization	-The assessment of proprioceptive functions during epidural electrical stimulation, performed in humans, was performed randomizing both the sequence of the tested stimulation parameters and the sequence of imposed passive movements. -The assessments of EES-induced responses during passive joint movements, performed in humans and rats, were performed by randomizing the sequence of the tested stimulation parameters. -The experiments on continuous EES during treadmill locomotion, performed in humans and rats, were performed by randomizing the sequence of the tested stimulation parameters.
Blinding	The investigators were not blinded to tested conditions.

Reporting for specific materials, systems and methods

Materials & experimental systems

n/a	Involved in the study
☒	☐ Unique biological materials
☒	☐ Antibodies
☒	☐ Eukaryotic cell lines
☒	☐ Palaeontology
☐	☒ Animals and other organisms
☐	☒ Human research participants

Methods

n/a	Involved in the study
☒	☐ ChIP-seq
☒	☐ Flow cytometry
☒	☐ MRI-based neuroimaging

Animals and other organisms

Policy information about studies involving animals; ARRIVE guidelines recommended for reporting animal research

Laboratory animals	Experiments in animals were conducted in: - Female Lewis rats, 11 weeks old. - Female Long-Evans rats, 11 weeks old.
Wild animals	The study did not involve wild animals.

Field-collected samples	The study did not involve samples collected from the field.

Human research participants

Policy information about studies involving human research participants

Population characteristics	Three male individuals, aged 28-47 y, all with a traumatic cervical spinal cord injury participated in the study. All participants had completed standard of care rehabilitation following their injury and were in a chronic state, 4-6 y post-injury. All displayed low motor scores in the lower limbs or complete motor paralysis, which bound them to a wheelchair.
Recruitment	Participant recruitment was done via the clinicaltrial.gov website where the principal investigators' contact details were disclosed (NCT02936453). Patients and physicians contacted them directly to communicate their interest to participate or to refer a patient to the STIMO study. The clinical study nurse communicated with the patients or the referring physician and reviewed the clinical status of the patient for compliance with the inclusion and exclusion criteria listed below. Patients meeting the inclusion criteria were given the study's flyer and the informed consent form to understand further their implications and involvement within this clinical study. The participants' selection was also based on their ability to live independently and their autonomy in their daily living activities. Inclusion Criteria: - Age 18-65 (women or men) - Incomplete SCI graded as AIS C & D - Level of lesion: T10 and above, based on AIS level determination by the PI, with preservation of conus function - The intact distance between the cone and the lesion must be at least 60mm - Focal spinal cord disorder caused by either trauma or epidural, subdural or intramedullary bleeding - Minimum 12 months post-injury - Completed in-patient rehabilitation program - Able to stand with walker or 2 crutches - Stable medical and physical condition as considered by Investigators - Adequate care-giver support and access to appropriate medical care in patient's home community - Agree to comply in good faith with all conditions of the study and to attend all required study training and visits - Must participate in two training sessions before enrolment - Must provide and sign Informed Consent prior to any study related procedures Exclusion Criteria: - Limitation of walking function based on accompanying (CNS) disorders (systemic malignant disorders, cardiovascular disorders restricting physical training, peripheral nerve disorders) - History of significant autonomic dysreflexia - Cognitive/brain damage - Epilepsy - Patient who uses an intrathecal Baclofen pump. - Patient who has any active implanted cardiac device such as pacemaker or defibrillator. - Patient who has any indication that would require diathermy. - Patient who has any indication that would require MRI. - Patient that have an increased risk for defibrillation - Severe joint contractures disabling or restricting lower limb movements. - Haematological disorders with increased risk for surgical interventions (increased risk of haemorrhagic events). - Participation in another locomotor training study. - Congenital or acquired lower limb abnormalities (affection of joints and bone). - Women who are pregnant (pregnancy test obligatory for woman of childbearing potential) or breast feeding or not willing to take contraception. - Known or suspected non-compliance, drug or alcohol abuse. - Spinal cord lesion due to either a neurodegenerative disease or a tumour. - Patient has other anatomic or co-morbid conditions that, in the investigator's opinion, could limit the patient's ability to participate in the study or to comply with follow-up requirements, or impact the scientific soundness of the study results. - Patient is unlikely to survive the protocol follow-up period of 12 months.